Thermodynamic Properties for 1-Hexene – Measurements and Modeling

Benjamin Betken,[a*] Robin Beckmüller,[a] Muhammad Ali Javed,[b,c] Elmar Baumhögger,[d] Roland Span[a], Jadran Vrabec,[b] Monika Thol[a]

[a]*Ruhr University Bochum, Thermodynamics, Universitätsstraße 150, 44801 Bochum, Germany*

[b]*Technical University of Berlin, Thermodynamics and Process Engineering, Ernst-Reuter-Platz 1, 10587 Berlin, Germany*

[c] *Chemnitz University of Technology, Reichenhainer Str. 70, 09126 Chemnitz, Germany*

[d] *University of Paderborn, Thermodynamics and Energy Technology, Warburger Straße 100, 33098 Paderborn, Germany*

[*]corresponding author: benjamin.betken@thermo.rub.de

Abstract

A fundamental equation of state is presented for 1-hexene. It is explicit in the reduced Helmholtz energy and depends on the independent variables temperature and density. It is valid in the fluid region at temperatures from the triple-point temperature T_{tr} = 133.39 K to T_{max} = 535 K with a maximum pressure of p_{max} = 245 MPa. All thermodynamic properties can be determined from the Helmholtz energy and its derivatives with respect to temperature and density. The equation of state is validated by comparison with experimental data, along with an assessment of correct physical and extrapolation behavior. The available data base is further extended by measurements of the homogeneous density with a vibrating-tube densimeter in the temperature range from 300 K to 362 K and pressures of up to 92 MPa. Speed of sound measurements are conducted with two independent apparatuses at temperatures of 215 K and 500 K and pressures of up to 151 MPa, applying the double-path-length pulse-echo technique.

Keywords: equation of state, Helmholtz energy, 1-hexene, experimental data, density, speed of sound

1. Introduction

Precise knowledge of thermodynamic properties of fluids is an essential basis for the efficient design of cost- or energy-intensive processes, especially in chemical engineering and energy technologies. Although the expansion of renewable energies has been decided and driven forward in recent years, natural gas will continue to play a significant role in the energy supply in Germany and Europe in the near future. In the course of the diversification of supply structures, suitable models must be available for the design of natural gas process chains, as well as for billing. For this purpose, accurate thermodynamic property models become increasingly relevant in technical applications. Today, the most accurate models are equations of state in terms of the Helmholtz energy, which are empirically adjusted to experimental data. Ideally, these equations reproduce the measurements within their experimental uncertainty. Thus, they allow for the calculation of thermodynamic properties with high accuracy in the entire fluid state region, provided that there are sufficient experimental data of good quality available.

The GERG-2008 [1] wide-range equation of state is the ISO standard [2] for the calculation of thermodynamic properties of natural gases. It comprises 21 typical natural gas components and was mainly developed for the calculation of thermodynamic properties under pipeline conditions. In the last decade, many projects have been initiated to modify and improve this equation for other purposes. This resulted, for example, in the EOS-CG [3] for the precise description of CO_2-rich mixtures, the EOS-LNG [4] for a more accurate calculation of liquefied natural-gas properties, or modified equations for hydrogen-rich mixtures [5]. All these efforts are still subject to ongoing research. However, none of these equations considers mixtures containing alkenes, such as pentene, hexene, or heptene. This is mainly due to the lack of corresponding pure-fluid equations of state, which are required for the development of mixture models. To meet this demand, a fundamental equation of state in terms of the Helmholtz energy for 1-hexene is presented here, which can be used for the extension of current models to mixtures containing alkenes. The basis for the development of such an equation of state is the availability of sufficient and accurate experimental data. In this context, the density at homogeneous states, the speed of sound at homogeneous states, and the vapor pressure are the most important property types.

Table 1: Thermodynamic properties of 1-hexene and the gas constant.

Physical property	Symbol	Value	Unit	Reference
Critical temperature	T_c	504.00	K	Gude and Teja [6]
Critical density	ρ_c	2.83	mol·dm^{-3}	This Work
Critical pressure	p_c	3.06297	MPa	This Work
Normal boiling point temperature	T_B	336.61	K	This Work
Triple point temperature	T_{tr}	133.39	K	McCullough et al. [7]
Triple point density, liquid	$\rho_{tr,liq}$	9.738	mol·dm^{-3}	This Work
Molar mass	M	84.15948	g·mol^{-1}	Wieser and Berglund [8]
Gas constant	R	8.314462618	J·mol^{-1}·K^{-1}	Tiesinga et al. [9]

Table 2: Specification of the materials and their suppliers.

chemical name	chemical formula	CAS no.	source	mass fraction purity[a]	purification method
propane	C_3H_8	74-98-6	Sigma-Aldrich	0.9950	none
water	H_2O	7732-18-5	Sigma-Aldrich	0.9999	none
1-hexene	C_6H_{12}	592-41-6	Acros Organics	0.9940	none

[a] Purities are given as stated by the suppliers.

A literature search showed that the density is sufficiently characterized, but only few speed of sound data are available. However, a closer analysis of the available density data showed contradictory trends, especially at elevated pressures. In order to improve the data situation, new density and speed of sound measurements were, thus, carried out in the liquid state region.

2. 1-Hexene

1-Hexene is a linear and unbranched isomer of hexene, an unsaturated hydrocarbon from the homologous series of alkenes with the chemical formula C_6H_{12}. It is listed under the international designation standard CAS number 592-41-6. The characteristic carbon-carbon double bond of alkenes is located between the first and second carbon atoms. Under normal conditions, 1-hexene is a colorless liquid with a gasoline-like smell. At higher concentrations it has a narcotic effect for humans and upon prolonged exposure it is lethal. 1-Hexene is highly flammable and forms explosive mixtures with air at ambient temperature. In water, 1-hexene is practically insoluble, but classified to be very toxic to aquatic life [10]. Alkenes in general can be produced, for example, by cracking petroleum fractions or via hydrogenation of alkynes. For linear alkenes in particular, catalytic oligomerization of ethene to higher hydrocarbons is applied [11]. Among others, 1-hexene is used as an additive in fuels and lubricants or as a co-monomer in the production of polyethylene. It is also an intermediate product in the chemical industry [12,13]. The thermodynamic properties of 1-hexene relevant to this work are listed in Table 1.

3. Experiment

3.1. Materials

Specifications of the chemicals used in the present work and their suppliers are provided in Table 2. The chemicals were purchased at high purity and before filling into the apparatus, they were degassed to remove volatile impurities. The degassing procedure was performed in an evacuated chamber at ambient temperature for about two hours with repeated renewal of the vacuum every 15 minutes.

3.2. Apparatus 1

To simultaneously measure the density and the speed of sound of 1-hexene, an apparatus was used in which a densimeter and an acoustic cell are combined [14]. A schematic of this apparatus is provided in Figure 1. The temperature was specified with a thermostat (Huber CC415) in which water was used as a heat transfer medium. It was circulated around the pressure vessels of the densimeter and the acoustic cell to maintain the temperature of the sample fluid within 0.01 K. The pressure was applied with a hand-driven pump (HIP 50-6-15) and measured with a transducer (Keller-PAA-33X). The apparatus was evacuated for about 2 h before filling with the sample fluid.

3.2.1. Density measurement with apparatus 1

The density of 1-hexene was measured with a U-shaped vibrating-tube densimeter (Anton Paar, DMA HPM), described in detail by Javed et al. [14]. This device has two parts, a measurement cell and an interface module. The sample fluid was filled into the densimeter, which oscillates with a period depending on the state of the fluid. The oscillation period of the vibrating-tube and the temperature of the sample fluid were measured with the built-in interface

module. The density can then be obtained from a function of temperature T, pressure p and oscillation period s,

$$\rho = f(T, p, s). \tag{1}$$

Before measuring the density, the apparatus was calibrated according to a method suggested by Anton Paar [15].

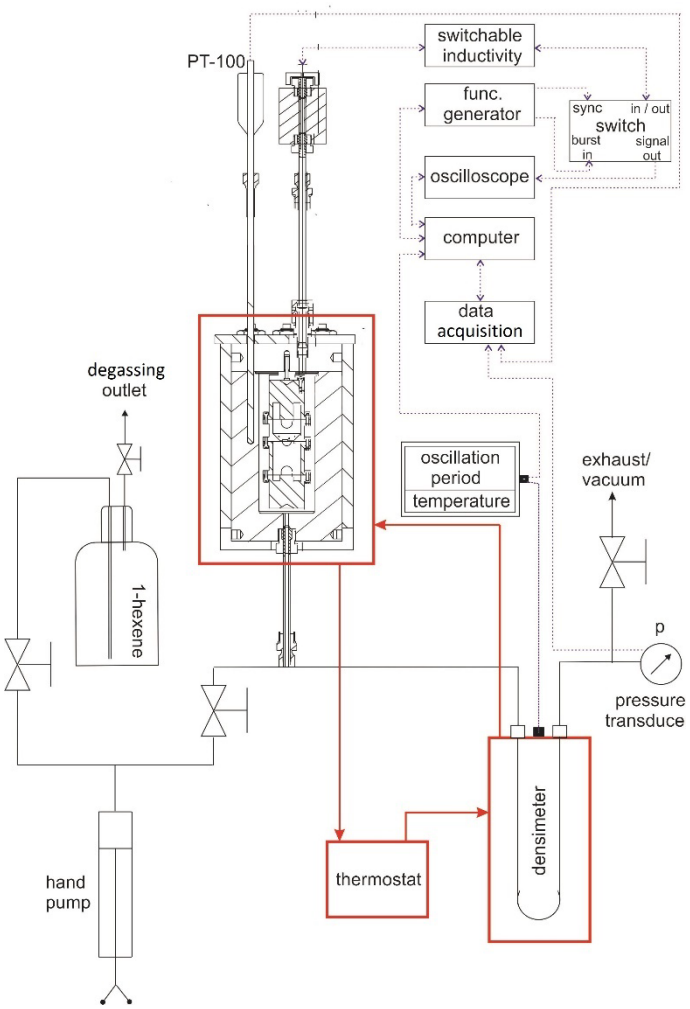

Figure 1. Schematic of apparatus 1 to simultaneously measure the density and speed of sound of 1-hexene.

For this purpose, propane and water were chosen as calibration fluids because their densities are well-known from reference quality Helmholtz energy equations of state of Lemmon et al. [16] and Wagner and Pruß [17]. Moreover, these fluids cover the entire density range of 1-hexene. For calibrating the densimeter, the density of the calibration fluids was calculated at different state points with the corresponding equations of state. The oscillation period of the densimeter at those state points was also measured for the calibration fluids, after filling them into the apparatus. A Legendre polynomial equation considering the individual parameters (T, p, and s) and their possible combinations was fitted to the density data of the calibration fluids. After excluding terms with weak contributions or high uncertainties, a third-order equation with ten coefficients was found

$$\begin{aligned}\rho = a + b_1\underline{T} + c_1\underline{p} + d_1\underline{s} + b_2\frac{(3\underline{T}^2-1)}{2} \\ + d_2\frac{(3\underline{s}^2-1)}{2} + b_1d_1\underline{T}\underline{s} \\ + b_1d_2\underline{T}\frac{(3\underline{s}^2-1)}{2} \\ + c_1d_2\underline{p}\frac{(3\underline{s}^2-1)}{2} + b_1c_1d_1\underline{T}\underline{p}\underline{s}.\end{aligned} \tag{2}$$

The coefficients a, b_i, c_i, and d_i were adjusted to the calibration data of both reference fluids. $\underline{T}$, $\underline{p}$ and $\underline{s}$ are the scaled temperature, pressure, and oscillation period, which were used to enhance the performance of Legendre polynomial equation

$$\underline{y} = \frac{y - \bar{y}}{\delta y}, \tag{3}$$

where $\bar{y}$ is the mean value of the corresponding variable and δy is the scaling span. The parameters of Eqs. (2) and (3) are listed in Table 3.

Table 3: Parameters of the calibration Eqs. (2) and (3) for the density measurement.

parameter	value	unit
a	750.0756	-
b_1	−359.6746	-
c_1	−4.9587	-
d_1	767.7276	-
b_2	−2.7453	-
d_2	1.4900	-
b_1d_1	−14.0967	-
b_1d_2	2.0918	-
c_1d_2	−3.6169	-
$b_1c_1d_1$	4.2310	-
$\bar{T}$	57.077	°C
δT	80	°C
$\bar{p}$	460.59	bar
δp	470	bar
$\bar{s}$	2646.468	µs
δs	60	µs

For measuring the density, 1-hexene was filled into the densimeter and the oscillation period was measured along four isotherms, i.e., 300 K, 323 K, 350 K, and 362 K, in the pressure range between 0.1 MPa and 91 MPa. The measured values of T, p, and s were used in Eq. (2) to calculate the density of 1-hexene.

Table 4: Density ρ of 1-hexene in the homogeneous liquid phase measured with apparatus 1 as a function of temperature T and pressure p, where U_ρ is the expanded uncertainty.[a]

T/K	p/MPa	ρ/(kg·m^{-3})	U_ρ/(kg·m^{-3})	T/K	p/MPa	ρ/(kg·m^{-3})	U_ρ/(kg·m^{-3})
299.9	0.09	666.4	1.1	350.5	1.20	618.1	1.1
299.9	1.28	667.7	1.0	350.5	4.98	624.6	1.1
299.9	5.11	672.0	1.0	350.5	9.80	632.0	1.0
300.0	10.08	677.2	1.0	350.4	17.32	642.2	1.0
299.9	18.87	685.6	1.0	350.5	22.22	648.2	1.0
299.9	29.03	694.3	1.0	350.5	31.35	658.2	1.0
300.0	51.32	710.7	1.0	350.5	50.68	676.1	1.0
299.9	69.53	722.2	1.0	350.5	70.64	691.4	1.0
300.0	89.35	733.4	1.0	350.5	90.76	704.6	1.0
322.8	0.19	644.5	1.1	362.3	0.24	603.4	1.1
322.8	1.11	645.8	1.1	362.3	1.09	605.2	1.1
322.8	5.23	651.3	1.0	362.3	4.61	612.1	1.1
322.8	10.77	658.1	1.0	362.3	5.09	612.9	1.1
322.8	15.33	663.3	1.0	362.3	9.68	620.8	1.0
322.8	21.70	669.9	1.0	362.3	11.40	623.5	1.0
322.8	31.11	678.8	1.0	362.3	21.03	637.1	1.0
322.8	51.40	695.2	1.0	362.3	30.66	648.5	1.0
322.8	70.44	708.2	1.0	362.3	50.43	667.9	1.0
322.8	91.22	720.7	1.0	362.3	70.56	684.1	1.0
350.5	0.18	616.2	1.1	362.3	90.73	697.9	1.0

[a] U_ρ is the expanded uncertainty of the density at a confidence level of 95 % (k = 2), composed of standard uncertainties of temperature u_T = 0.1 K, pressure u_p = 0.02 MPa, oscillation period u_s = 0.015 µs, and calibration u_{cal} = 0.5 kg·m^{-3}.

The density data of 1-hexene are listed in Table 4. The expanded uncertainty U_ρ is also provided assuming a coverage factor k = 2, which leads to a level of confidence of 95 %. The expanded uncertainty was calculated applying the Gaussian error propagation law

$$U_\rho = k\left[\left(\left(\frac{\partial\rho}{\partial T}\right)_{p,s}u_T\right)^2 + \left(\left(\frac{\partial\rho}{\partial p}\right)_{T,s}u_p\right)^2 + \left(\left(\frac{\partial\rho}{\partial s}\right)_{T,p}u_s\right)^2 + {u_{\mathrm{cal}}}^2\right]^{\frac{1}{2}}, \quad (4)$$

where U_ρ is the expanded uncertainty of density at a confidence level of 95 % (k = 2), composed of standard uncertainties of temperature u_T = 0.1 K, pressure u_p = 0.02 MPa, oscillation period u_s = 0.015 µs, and calibration u_{cal} = 0.5 kg m^{-3}.

3.2.2. Speed of sound measurement with apparatus 1

The speed of sound of 1-hexene was also measured with apparatus 1, covering the temperature range between 300 K and 362 K with a pressure of up to 91 MPa.

For measuring the speed of sound of 1-hexene, a double-path-length pulse-echo technique was implemented. For this purpose, an 8 MHz piezoelectric quartz crystal was used as acoustic transducer, which was placed between two metallic reflectors, mounted at different distances [14,18]. To measure the speed of sound, the quartz crystal was excited with an electric burst signal of eight periods. Consequently, two sound waves propagated through the sample fluid in opposite directions. After reflection, these sound waves were received by the quartz crystal again, which also acts as a sound receiver. The sampled signals were analyzed with a computer-controlled oscilloscope.

Neglecting the diffraction effect, the speed of sound w was calculated from the path length difference $2\Delta L$ and the delay in the time of flight Δt

$$w = \frac{2\Delta L}{\Delta t}. \quad (5)$$

Because the acoustic cell is made of steel, the path length of the acoustic cell changes with temperature and pressure. This effect was considered according to

$$\Delta L_{T,p} = \Delta L_{T_0,p_0}\left(1 + \alpha(T - T_0) + \frac{1}{E}(1 - 2\upsilon)(p_0 - p)\right). \quad (6)$$

Therein, $\Delta L_{T_0,\ p_0}$ is the calibrated path length at T_0 = 300 K and p_0 = 1 MPa, α the linear thermal expansion coefficient, E the elastic modulus and υ the Poisson number of the stainless steel 1.4571, provided by its supplier (Thyssen-Krupp Materials International) [18]. The path length of the acoustic cell was calibrated with water [14].

Table 5: Speed of sound w of 1-hexene in the homogeneous liquid phase measured with apparatus 1 as a function of temperature T and pressure p, where U_w is the expanded uncertainty.[a]

T/K	p/MPa	w/(m·s^{-1})	U_w/(m·s^{-1})	T/K	p/MPa	w/(m·s^{-1})	U_w/(m·s^{-1})
300.1	0.11	1057.9	1.0	349.7	0.19	837.3	0.8
300.1	1.28	1067.7	1.0	349.7	1.21	849.3	0.9
300.1	5.12	1098.4	1.0	349.7	4.99	890.4	0.8
300.1	10.10	1135.5	1.0	349.8	9.81	937.5	0.9
300.1	18.89	1195.2	1.0	349.8	22.23	1040.6	1.0
300.1	29.05	1257.1	1.1	349.8	31.36	1105.0	1.0
300.1	51.34	1374.0	1.2	349.8	50.69	1221.1	1.1
300.1	69.54	1456.3	1.3	349.8	70.65	1322.1	1.1
300.2	89.35	1536.0	1.3	349.8	90.77	1410.8	1.2
322.6	0.20	957.7	0.9	361.3	0.25	786.9	0.8
322.6	1.12	966.5	0.9	361.4	1.11	797.8	0.8
322.6	5.24	1004.2	0.9	361.4	5.10	844.8	0.8
322.6	10.79	1050.5	1.0	361.3	9.69	892.9	0.8
322.6	21.71	1130.6	1.0	361.4	21.04	993.2	0.9
322.6	31.12	1191.2	1.0	361.4	30.67	1064.7	1.0
322.6	51.40	1303.9	1.1	361.4	50.44	1188.0	1.0
322.6	70.45	1394.4	1.2	361.4	70.57	1292.4	1.1
322.6	91.22	1481.5	1.3	361.4	90.75	1383.1	1.2

[a] U_w is the expanded uncertainty of the speed of sound at a confidence level of 95 % (k = 2), composed of standard uncertainties of temperature u_T = 0.05 K, pressure u_p = 0.02 MPa, delay in time of flight $u_{\Delta t}$ = 0.002 µs, and path length difference $u_{\Delta L}$ = 7 µm.

The speed of sound data of 1-hexene along with their expanded uncertainty as a function of temperature and pressure measured with apparatus 1 are provided in Table 5. The overall expanded uncertainty U_w of the speed of sound measurement is composed of the relevant contributions due to standard uncertainties

$$U_w = k\left[\left(\left(\frac{\partial w}{\partial T}\right)_{p,\Delta L,\Delta t} u_T\right)^2 + \left(\left(\frac{\partial w}{\partial p}\right)_{T,\Delta L,\Delta t} u_p\right)^2 + \left(\left(\frac{\partial w}{\partial \Delta L}\right)_{T,p,\Delta t} u_{\Delta L}\right)^2 + \left(\left(\frac{\partial w}{\partial \Delta t}\right)_{T,p,\Delta L} u_{\Delta t}\right)^2\right]^{\frac{1}{2}}, \quad (7)$$

where U_w is the expanded uncertainty of speed of sound at a confidence level of 95 % (k = 2), composed of standard uncertainties of temperature u_T = 0.05 K, pressure u_p = 0.02 MPa, delay in time of flight $u_{\Delta t}$ = 0.002 µs, and path length difference $u_{\Delta L}$ = 7 µm.

3.2.3. Speed of sound measurement with apparatus 2

The speed of sound of 1-hexene was also measured with a second apparatus, which is based on the same pulse-echo technique as described in the previous section and a similar 8 MHz piezoelectric quartz crystal was used as acoustic transducer. However, this device can be applied to wider temperature and pressure ranges. The design and schematic of apparatus 2 was provided and discussed in detail by Javed et al. [19]. With this apparatus, the speed of sound of 1-hexene was measured along seven isotherms, covering a temperature range between 216 K and 500 K for pressures of up to 151 MPa. The speed of sound data with expanded experimental uncertainties at a confidence level of 95% (k = 2) are listed in Table 6. The data were measured between 557.3 m·s^{-1} and 1788.8 m·s^{-1} in the liquid and supercritical regions.

Table 6: Speed of sound w of 1-hexene in the homogeneous liquid phase measured with apparatus 2 as a function of temperature T and pressure p, where U_w is the expanded uncertainty.[a]

T/K	p/MPa	w/(m·s^{-1})	U_w/(m·s^{-1})	T/K	p/MPa	w/(m·s^{-1})	U_w/(m·s^{-1})
215.86	0.102	1461.2	1.3	350.08	4.987	889.0	0.7
215.86	0.520	1463.5	1.3	350.08	8.009	919.1	0.7
215.84	1.013	1466.0	1.3	350.08	9.938	937.2	0.7
215.85	2.015	1471.0	1.3	350.08	20.113	1022.8	0.8
215.85	5.054	1486.1	1.3	350.07	40.404	1160.2	0.9
215.85	8.090	1500.8	1.3	350.07	60.090	1268.6	1.0
215.85	9.932	1509.6	1.3	350.08	79.948	1362.4	1.0
215.85	20.203	1556.5	1.3	350.08	99.807	1445.4	1.1
215.85	40.084	1638.9	1.3	350.08	125.439	1540.7	1.3
215.86	60.127	1713.3	1.3	350.08	132.597	1565.5	1.3
215.87	69.981	1747.2	1.3	350.08	151.303	1626.9	1.3
215.86	80.088	1780.7	1.3	400.10	0.612	619.5	0.5
215.86	82.584	1788.8	1.3	400.11	1.067	628.2	0.5
249.98	0.109	1294.6	1.0	400.12	2.005	644.0	0.5

250.00	0.498	1296.9	1.0	400.14	5.004	691.0	0.5
250.01	1.254	1301.5	1.0	400.14	8.001	732.0	0.5
250.00	2.032	1306.2	1.0	400.14	9.944	756.2	0.6
250.00	4.959	1323.5	1.0	400.08	20.026	863.2	0.7
250.00	8.059	1341.4	1.0	400.08	40.120	1022.7	0.8
250.00	9.938	1351.9	1.0	400.08	60.005	1145.1	0.9
250.00	20.018	1405.5	1.1	400.08	80.016	1248.2	0.9
250.01	40.080	1500.5	1.2	400.08	99.723	1336.8	1.0
250.01	60.074	1583.6	1.2	400.07	125.887	1440.2	1.2
250.01	80.027	1658.1	1.3	400.07	150.981	1528.5	1.3
249.99	95.178	1710.3	1.3	449.97	8.021	557.3	0.4
299.97	0.495	1062.3	0.8	449.97	9.970	590.6	0.4
299.97	1.055	1067.0	0.8	449.95	20.011	723.1	0.6
299.97	2.017	1074.9	0.8	449.95	40.052	905.9	0.7
299.97	5.039	1098.8	0.8	449.97	60.007	1040.6	0.8
299.97	8.019	1121.4	0.8	449.97	80.020	1151.1	0.9
299.97	9.946	1135.4	0.9	449.97	99.896	1245.7	0.9
299.98	20.075	1203.8	0.9	449.97	126.165	1354.7	1.1
299.98	40.064	1318.6	1.0	449.97	151.334	1446.9	1.2
299.97	60.013	1415.6	1.1	499.97	19.986	605.6	0.5
299.97	79.352	1499.0	1.2	499.97	40.010	810.2	0.6
299.97	99.643	1576.2	1.2	499.98	59.998	954.9	0.7
350.08	0.206	836.7	0.6	499.98	80.004	1071.5	0.8
350.08	0.514	840.0	0.6	499.97	126.135	1285.3	1.1
350.08	0.997	845.6	0.6	499.97	151.322	1380.5	1.2
350.08	1.996	857.0	0.6				

[a] U_w is the expanded uncertainty of the speed of sound at a confidence level of 95 % (k = 2), composed of standard uncertainties of temperature u_T = 0.02 K, pressure u_p = 0.002 MPa for p < 10 MPa, 0.02 MPa for p < 100 MPa and 0.06 MPa for p ≥ 100 MPa, delay in time of flight $u_{\Delta t}$ = 0.002 µs, and path length difference $u_{\Delta L}$ = 7 µm.

U_w is the expanded uncertainty of the speed of sound at a confidence level of 95% (k = 2), composed of standard uncertainties of temperature u_T = 0.02 K, pressure u_p = 0.002 MPa for p < 10 MPa, 0.02 MPa for p < 100 MPa and 0.06 MPa for $p \geq 100$ MPa, delay in time of flight $u_{\Delta t}$ = 0.002 µs, and path length difference $u_{\Delta L}$ = 7 µm.

4. Equation of State for 1-Hexene

The equation of state presented in this work is explicit in terms of the Helmholtz energy a, which can be transformed into its dimensionless form α by the reducing parameters temperature T and gas constant R

$$\alpha(\tau, \delta) = \frac{a(T, \rho)}{RT}. \quad (8)$$

The independent variables temperature T and molar density ρ are transferred to the inverse reduced temperature τ and the reduced density δ, respectively, by means of the critical parameters T_c and ρ_c

$$\tau = \frac{T_c}{T} \text{ and } \delta = \frac{\rho}{\rho_c}. \quad (9)$$

For the critical properties of 1-hexene, 13 publications were found in the literature, as summarized in Table 7. Since the critical region is characterized by specific slopes and curvatures of the saturation lines and isolines, the critical parameters have a significant impact in this state region. Therefore, they have to be chosen carefully. An overview of available literature data for T_c and ρ_c and the critical parameters used in this work, can be found in Figure 2.

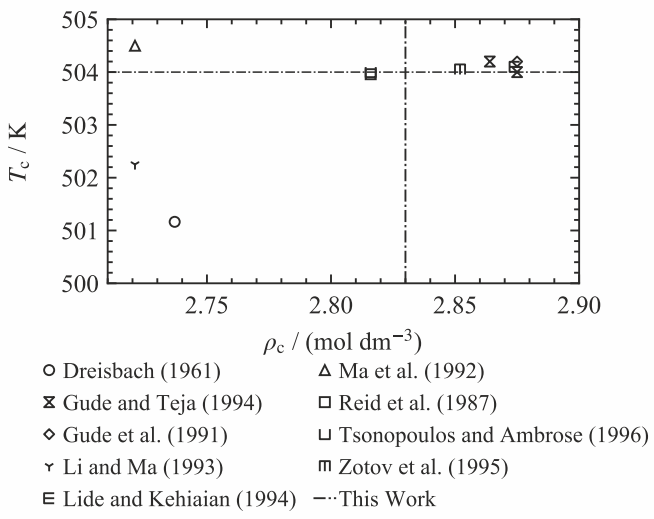

Figure 2. Selected literature data for the critical temperature T_c and critical density ρ_c. The dot-dashed lines represent the critical properties used in this work.

The critical temperature was set to T_c = 504.00 K according to Gude and Teja [6]. The critical density ρ_c = 2.83 mol·dm^{-3} was empirically determined during the fitting procedure. With this set of critical parameters, the representation of experimental density data was enhanced and reasonable behavior of the rectilinear diameter ρ_{RD} (cf. Sec. 6) was achieved. The reduced Helmholtz energy can be written as the sum of an ideal part α^o, which describes the behavior of the hypothetical ideal gas, and a residual part α^r, which takes the behavior of the real fluid into account

$$\alpha(\tau,\delta) = \alpha^{\mathrm{o}}(\tau,\delta) + \alpha^{\mathrm{r}}(\tau,\delta). \qquad (10)$$

Table 7: Literature data for the critical temperature T_c, critical pressure p_c and critical density ρ_c of 1-hexene. Units were converted to molar SI units and to the ITS-90 scale where necessary.

Reference	Year	T_c / K	p_c / MPa	ρ_c / (mol·dm^{-3})
Altschul [20]	1893	516.669	-	-
Herz [21]	1916	516.519	-	-
Ambrose et al. [22]	1960	503.995	-	-
Dreisbach [23]	1961	501.164	3.022	2.737
Kay and Young [24]	1974	503.16	3.212	-
Reid et al. [25]	1987	503.96	3.143	2.816
Gude et al. [26]	1991	504.2	3.206	2.875
Ma et al. [27]	1992	504.5	3.186	2.721
Li and Ma [28]	1993	502.25	3.339	2.721
		504.2	-	2.864
Gude and Teja [6]	1994	504	-	2.875
		504.8	3.206	-
Lide and Kehiaian [29]	1994	504.1	3.206	2.874
Zotov et al. [30]	1995	504.05	-	2.852
Tsonopoulos and Ambrose [31]	1996	504	3.21	2.816

Table 8: Parameters of the ideal part of the present equation of state, cf. Eq. (13).

k	m_k / -	θ_k / K
1	8.65	360
2	14.10	3534
3	21.90	1473
	c^{I}	c^{II}
	0.1361322645	5.9040396248

4.1. Ideal-Gas Contribution

The ideal part can be obtained from

$$\alpha^{\mathrm{o}}(\tau,\delta) = \int \left(\int -\frac{c_v^{\mathrm{o}}}{R\tau^2}\,\mathrm{d}\tau \right) \mathrm{d}\tau + \ln\left(\frac{\delta}{\delta_0}\right), \qquad (11)$$

by a twofold integration of the ideal gas isochoric heat capacity c_v^{o} with respect to temperature. The temperature dependence of c_v^{o} is given as follows

$$\frac{c_v^{\mathrm{o}}}{R} = n_0 + \sum_{k=1}^{K_{\mathrm{PE}}} m_k \left(\frac{\theta_k}{T}\right)^2 \frac{\exp\left(\frac{\theta_k}{T}\right)}{\left(\exp\left(\frac{\theta_k}{T}\right) - 1\right)^2}, \qquad (12)$$

where n_0 is determined by the number of the translational and external rotational degrees of freedom. Since every degree of freedom contributes $0.5 \cdot R$ to the isochoric heat capacity, $n_0 = 3$ holds for non-linear molecules like 1-hexene. The sum goes over the so-called Planck-Einstein functions, which were introduced to consider intramolecular vibrations. The parameters Θ_k and m_k can be determined by means of statistical thermodynamics. However, for the development of this equation, they were empirically adjusted to ideal gas isobaric heat capacity data from the literature. Eqs. (11) and (12) finally result in the following functional form of the reduced ideal Helmholtz energy

$$\alpha^{\mathrm{o}}(\tau,\delta) = c^{\mathrm{II}} + c^{\mathrm{I}}\tau + 3\ln(\tau) + \sum_{k=1}^{3} m_k \ln\left(1 - \exp\left(\frac{\theta_k}{T}\right)\right) + \ln(\delta). \qquad (13)$$

The integration constants c^{I} and c^{II} depend on the reference state, which can be chosen arbitrarily. In this case, the normal boiling point (T_B = 336.61 K) was chosen as reference state, where the enthalpy and entropy were set to zero for the saturated liquid at atmospheric pressure. The values of all parameters and integration constants according to Eq. (13) are listed in Table 8. In Figure 3, relative deviations between theoretically determined data of the ideal gas isobaric heat capacity c_p^{o} taken from Kilpatrick et al. [32] and values calculated with the present equation of state are plotted as a function of temperature.

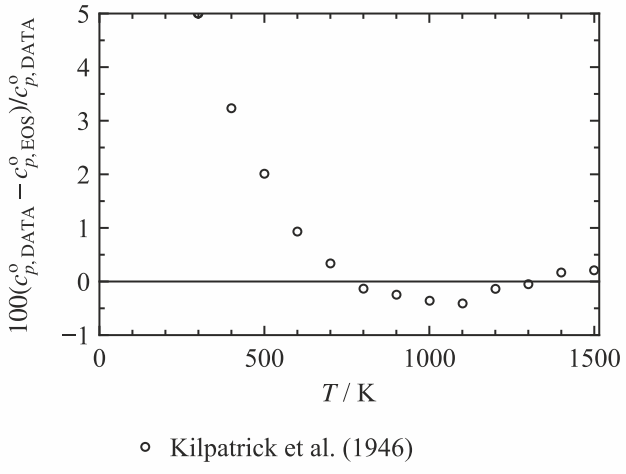

Figure 3. Relative deviations of ideal isobaric heat capacity data from the present equation of state.

The data deviate by up to 6.6 % from the present equation of state at temperatures below 500 K. Fitting them more accurately leads to a worse description of experimental data for the real fluid. Up to 500 K, experimental heat capacity and speed of sound data are available. Since the calculation of caloric properties always includes contributions of the ideal and residual part and both parts are fitted simultaneously, the parametrization of the ideal part is also affected by fitting heat capacity and speed of sound data. Since the experimental speed of sound data are of high accuracy, these data were preferred to the theoretically based c_p^0 data at temperatures $T < 600$ K. Thus, data of Kilpatrick et al. [32] were only fitted in temperature ranges where no other caloric data were available.

Table 9: Parameters of the residual part of the present equation of state according to Eq. (14).

i	n_i	t_i	d_i	p_i	η_i	β_i	γ_i	ε_i
1	0.04044199	1	4					
2	1.8522012	0.371	1					
3	−2.1391357	0.855	1					
4	−0.77947556	0.995	2					
5	0.21159454	0.553	3					
6	−3.3264005	1.31	1	2				
7	−1.0902532	2.3	3	2				
8	0.59957238	0.679	2	1				
9	−1.2866639	1.45	2	2				
10	−0.02127171	1.08	7	1				
11	3.9185489	0.751	1		−0.862	−0.766	1.193	0.765
12	−0.45724185	0.863	3		−1.09	−0.903	1.297	0.746
13	−0.82698194	0.67	2		−0.802	−0.714	1.11	0.728
14	−1.0764178	0.638	2		−1.14	−1.3	0.879	0.498
15	−0.002580659	0.677	1		−6.47	−212.14	1.09	0.912

4.2. Residual contribution

The residual part of the Helmholtz energy α^{r} takes into account the deviations of the real fluid due to intermolecular interactions. It consists of five polynomial, five exponential, and five Gaussian bell-shaped terms

$$\alpha^{\mathrm{r}}(\tau,\delta) = \sum_{i=1}^{5} n_i \delta^{d_i} \tau^{t_i} + \sum_{i=6}^{10} n_i \delta^{d_i} \tau^{t_i} \exp(-\delta^{p_i}) + \sum_{i=11}^{15} n_i \delta^{d_i} \tau^{t_i} \exp(-\eta_i(\delta-\varepsilon_i)^2 - \beta_i(\tau-\gamma_i)^2). \quad (14)$$

The adjustable parameters n_i, t_i, η_i, ε_i, β_i and γ_i were empirically optimized using a non-linear fitting algorithm developed by Lemmon and Jacobsen [33]. The density exponents d_i and p_i are positive integers and were not adjusted, but defined on the basis of experience. The corresponding values are listed in Table 9.

4.3. Ancillary Equations

Saturation properties under vapor-liquid equilibrium cannot be directly calculated with the equation of state, but have to be determined iteratively applying the Maxwell criterion. To reduce computing time, ancillary equations (cf. Eqs. (15) to (17)) are supplied for the generation of starting values for the vapor pressure p_{v}, saturated liquid density ρ' and saturated vapor density ρ''

$$\ln\left(\frac{p_{\mathrm{v}}}{p_{\mathrm{c}}}\right) = \frac{T_{\mathrm{c}}}{T}\sum_{i=1}^{5} n_i \left(1-\frac{T}{T_{\mathrm{c}}}\right)^{k_i}, \quad (15)$$

$$\frac{\rho'}{\rho_{\mathrm{c}}} = 1 + \sum_{i=1}^{5} n_i \left(1-\frac{T}{T_{\mathrm{c}}}\right)^{k_i}, \quad (16)$$

$$\ln\left(\frac{\rho''}{\rho_{\mathrm{c}}}\right) = \sum_{i=1}^{6} n_i \left(1-\frac{T}{T_{\mathrm{c}}}\right)^{k_i}. \quad (17)$$

Table 10: Parameters of the ancillary equations for the vapor pressure p_{v}, saturated liquid density ρ', and saturated vapor density ρ'' (cf. Eqs. (15) to (17)).

i	p_{v}		ρ'		ρ''	
	n_i	k_i	n_i	k_i	n_i	k_i
1	−7.526	1	1.5987	0.29	−2.3518	0.33
2	2.924	1.5	1.1019	0.744	−5.7777	1.04
3	−2.8748	2.02	2.5409	5.68	−16.194	2.76
4	−3.584	4.45	−5.0722	6.76	−48.539	5.98
5	−3.229	17.8	3.0936	7.66	−81.266	11.91
6	-	-	-	-	−174.12	21.4

The parameters of Eqs. (15) to (17) are listed in Table 10. Figure 4 shows the relative deviations between the ancillary equations and the equation of state plotted as a function of temperature. Deviations of the vapor pressure do not exceed 0.03 %. The ancillary equations for the saturated densities

deviate within 0.013 % from the equation of state over a wide temperature range. Close to the critical temperature, the deviations increase up to 0.028 % for ρ'' and 0.045 % for ρ'.

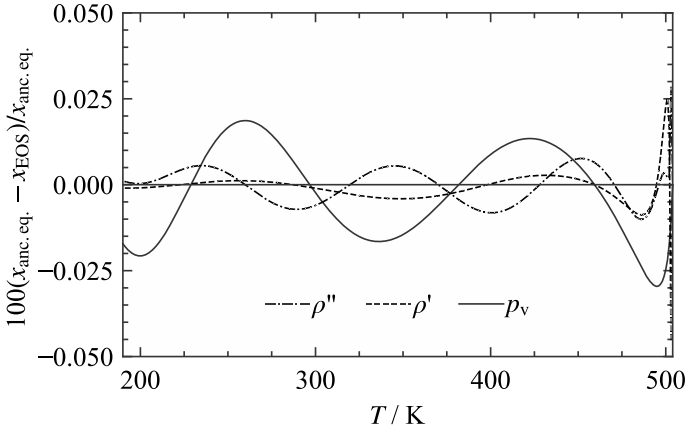

Figure 4. Percentage deviations of vapor pressure p_v, saturated liquid density ρ', and saturated vapor density ρ'' calculated with the ancillary equations from the present equation of state as a function of temperature.

5. Comparison of the Equation of State to Experimental Data

As mentioned in Sec. 4.2, a non-linear fitting algorithm developed by Lemmon and Jacobsen [33] was used to adjust the parameters of Eqs. (13) and (14) and the critical density. The fitting algorithm varies the parameters in order to minimize the weighted sum of squares (SSQ) of the relative deviation between selected experimental data and the equation of state

$$\mathrm{SSQ} = \sum W_x F_x^2, \tag{18}$$

where F is the relative deviation of each data point

$$F_x = \frac{x_{\mathrm{DATA}} - x_{\mathrm{EOS}}}{x_{\mathrm{DATA}}}, \tag{19}$$

and x can be any thermodynamic property. W is an individual weight of selected data points chosen by the correlator. In addition to fitting experimental data, mathematical constraints can be applied to define slopes, curvatures, or higher derivatives of different thermodynamic properties, as well as inequality criteria or limiting bounds for the values of the equation parameters. Especially in regions where no experimental data are available, constraints are a powerful tool to achieve a reasonable extrapolation and physical behavior. The goal of the adjustment process was to achieve a reasonable physical behavior combined with an accurate representation of the available experimental data, ideally within their experimental uncertainty. For the evaluation of the equation of state, the relative deviation of each data point and the average absolute relative deviations (AARD) of each dataset according to Eq. (20) are considered, along with a visual assessment of different thermodynamic properties and derivatives over a wide temperature and pressure range

$$\mathrm{AARD} = \frac{100}{N} \sum |F_x|, \tag{20}$$

where N is the number of data points for each dataset.

Table 11: Available experimental data and number of fitted data points for each property.

Property	available data points	fitted data points
$p\rho T$	1058	20
ρ'	31	-
ρ''	4	-
B	17	3
p_v	247	8
h_{vap}	4	-
c_p^0	14	5
c_p	109	-
c_σ	31	8
w	310	32
Total	1825	76

Depending on the property, the AARD of the datasets were determined separately for different state regions. The homogeneous region was separated into gas phase ($T < T_c$ and $\rho < \rho_c$), liquid phase ($T < T_c$ and $\rho > \rho_c$), critical region ($0.98 < T/T_c < 1.1$; $0.7 < \rho/\rho_c < 1.4$), and supercritical region ($T > T_c$). The supercritical region was further separated into low-density (LD: $\rho/\rho_c < 0.6$), medium-density (MD: $0.6 \le \rho/\rho_c \le 1.5$), and high-density range (HD: $\rho/\rho_c > 1.5$). Thermal saturation data were categorized into a low-temperature (LT: $T/T_c < 0.6$), medium-temperature (MT: $0.6 \le T/T_c \le 0.98$) and high-temperature (HT: $T/T_c > 0.98$) range. In addition to the experimental data presented in Sec. 3, the data base for developing the equation of state was compiled from 120 publications. A summary of the available experimental data and the number of fitted data points for each property is given in Table 11. Most of these data were measured in the homogeneous liquid phase, cf. Figure 5.

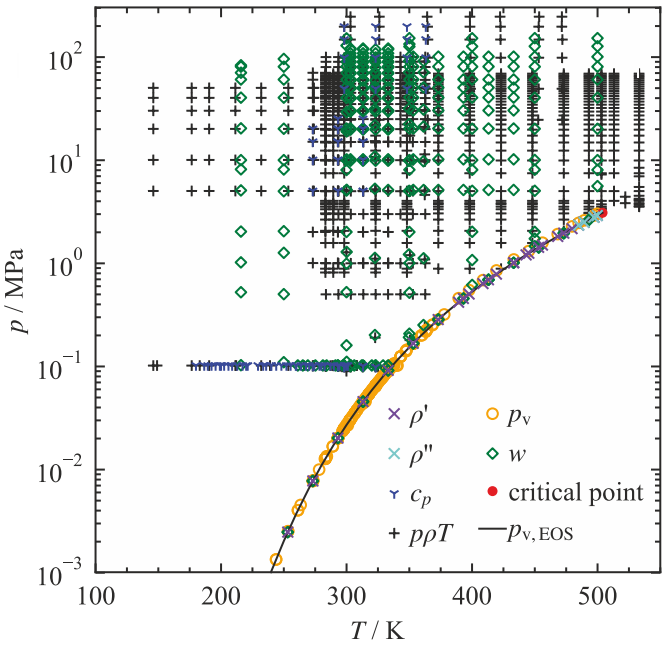

Figure 5. p,T-diagram showing the available experimental saturated liquid density (ρ'), saturated vapor density (ρ''), isobaric heat capacity (c_p), homogeneous density ($p\rho T$), vapor pressure (p_v), and speed of sound (w) data for 1-hexene. Additionally, the critical point and vapor pressure curve ($p_{v,EOS}$) calculated with the present equation of state are illustrated.

5.1. Density

The most comprehensively investigated property is the density, covering a broad state range of the liquid phase up to the supercritical region at temperatures between 146 K and 534 K and pressures of up to 245 MPa. In total, 1058 data points were available, including the data presented in Sec. 3.2.1 and literature data compiled from 64 publications. The AARD of each dataset are listed in Table 12, together with the corresponding temperature and pressure range. Saturated liquid and saturated vapor densities were only available to a limited extent and no data for the homogeneous vapor phase were found.

Vega-Maza et al. [34] and Torín-Ollarves et al. [35] both measured the liquid phase density in a temperature range from 273 K to 333 K at pressures of up to 70 MPa. It should be noted here, that the temperature of the lowest isotherm of the dataset of Vega-Maza et al. [34] was corrected from 283.15 K to 273.15 K in the present work. The corresponding density data are in remarkably good agreement with the density data at T = 273.15 K of Torín-Ollarves et al. [35] Therefore, we assumed this was a typographical error. Both research groups carried out their measurements with the same vibrating-tube densimeter (Anton Paar HPM). The calibration was done according to the method developed by Lagourette et al. [36], with measurements of water and the evacuated apparatus as reference. Reference values for the density of water were calculated with the equation of state of Wagner and Pruß [17]. The standard uncertainties for density, temperature, and pressure are stated in both publications as 3.5 10^{-4} g·cm^{-3}, 10 mK, and 0.02 % (k = 1), respectively. Applying the Gaussian error propagation law, the expanded combined uncertainty for density yields 0.7 kg·m^{-3} (k = 2), which corresponds to relative expanded combined uncertainties between 0.095 % and 0.11 % (k = 2). The purity of the sample used by Vega-Maza et al. [34] is stated as 99.5 mass % and of the sample used by Torín-Ollarves et al. [35] is stated as 99.7 mol %. Densities measured by Torín-Ollarves et al. [35] are slightly smaller, but both datasets coincide within their expanded uncertainty. The datasets of Vega-Maza et al. [34] and Torín-Ollarves et al. [35] are reproduced with an AARD of 0.02 % and 0.072 %, respectively, with the present equation of state and, thus, within the experimental uncertainty.

Table 12: Average absolute relative deviations (AARD) of homogeneous density data from the present equation of state.

				AARD / %					
Reference	N	$(T_{min} - T_{max})$ / K	$(p_{min} - p_{max})$ / MPa	liq.	crit.	LD	MD	HD	Overall
Abas-Zade et al. (1970) [37]	19	473 - 534	3.0 – 8.5	0.76	6.2	-	10	6.4	8.6
Abala et al. (2021) [38]	1	298.15	0.1	0.087	-	-	-	-	0.087
Aicart et al. (1995) [39]	1	298.15	0.101325	0.055	-	-	-	-	0.055
Belhadj et al .(2022) [40]	3	293 – 304	0.1	0.054	-	-	-	-	0.054
Bourguel (1927) [41]	1	287.14	0.101325	0.77	-	-	-	-	0.77
Bravo et al. (1991) [42]	1	298.15	0.101325	0.006	-	-	-	-	0.006
Bravo et al. (1992) [43]	1	308.15	0.101325	0.002	-	-	-	-	0.002
Campbell and Eby (1941) [44]	2	293.14	0.101325	0.17	-	-	-	-	0.17
Campbell and O'Connor (1939) [45]	1	293.14	0.098925	0.13	-	-	-	-	0.13
Chen and Liu (2013) [46]	1	298.15	0.101325	0.98	-	-	-	-	0.98
de Fré and Verhoeye (1976) [47]	1	298.14	0.101325	0.009	-	-	-	-	0.009
Desty and Fidler (1951) [48]	1	293.14	0.101325	0.02	-	-	-	-	0.02
Dojčanský et al. (1967) [49]	1	298.14	0.101325	0.29	-	-	-	-	0.29
Dreisbach (1961) [23]	3	293 - 304	0.101325	0.008	-	-	-	-	0.008
Fomina (1986) [50]	52	298 - 472	0.1 - 245	0.57	-	-	-	-	0.57
Forziati et al. (1950) [51]	3	293 - 304	0.101325	0.006	-	-	-	-	0.006
Garner et al. (1932) [52]	1	293.14	0.101325	0.51	-	-	-	-	0.51

Gee et al. (1986) [53]	5	149 - 267	0.101325	0.52	-	-	-	-	0.52
Geiseler and Pilz (1962) [54]	1	293.14	0.101325	0.48	-	-	-	-	0.48
Guseinov and Galandarov (1982) [55]	56	146 - 294	0.1 – 50.0	0.3	-	-	-	-	0.3
Hollenshead and Van Winkle (1966) [56]	1	298.14	0.101325	0.01	-	-	-	-	0.01
Jeffery and Vogel (1948) [57]	6	288 - 315	0.101325	1.1	-	-	-	-	1.1
Kerimov and Apaev (1972) [58]	493	283 - 534	0.1 – 68.8	0.27	2.5	-	0.75	0.37	0.31
Krollpfeiffer and Seebaum (1928) [59]	4	293.14	0.101325	2.5	-	-	-	-	2.5
Kudryavtseva et al. (1968) [60]	1	293.14	0.101325	0.005	-	-	-	-	0.005
Kudryavtseva et al. (1969) [61]	1	293.14	0.101325	0.004	-	-	-	-	0.004
Kudryavtseva et al. (1974) [62]	1	293.14	0.101325	0.011	-	-	-	-	0.011
Lesteva et al. (1979) [63]	2	293 - 314	0.101325	0.47	-	-	-	-	0.47
Letcher (1975) [64]	1	298.14	0.101325	0.056	-	-	-	-	0.056
Letcher (1977) [65]	1	298.14	0.101325	0.004	-	-	-	-	0.004
Letcher and Marsicano (1974) [66]	2	308 - 324	0.101325	0.031	-	-	-	-	0.031
Letcher and Reddy (2004) [67]	2	298.15	0.101325	0.19	-	-	-	-	0.19
Lide and Kehiaian (1994) [29]	1	298.15	0.101325	0.027	-	-	-	-	0.027
Lifi et al. (2021) [68]	1	298.15	0.1	0.012	-	-	-	-	0.012
Marrufo et al. (2009) [69]	1	298.15	0.101325	0.14	-	-	-	-	0.14
McCoubrey et al. (1951) [70]	1	336.62	0.101325	1.9	-	-	-	-	1.9
Mears et al. (1950) [71]	2	293 - 299	0.101325	0.009	-	-	-	-	0.009
Melikhov et al. (1991) [72]	1	293.15	0.101325	0.014	-	-	-	-	0.014
Nazmul Hasan (2010) [73]	1	298.15	0.101325	0.051	-	-	-	-	0.051
Ogorodnikov et al. (1961) [74]	1	293.14	0.101325	0.41	-	-	-	-	0.41
Ohlin et al. (2004) [75]	1	295	0.1	0.24	-	-	-	-	0.24
Pukinskii et al. (1982) [76]	1	293.14	0.101325	0.041	-	-	-	-	0.041
Reid et al. (1987) [25]	1	298.14	0.101325	0.006	-	-	-	-	0.006
Renon and Prausnitz (1968) [77]	1	298.14	0.101325	0.065	-	-	-	-	0.065
Sagdeev et al. (2014) [78]	29	298 – 473	0.1 – 245	0.54	-	-	-	-	0.54
Suryanarayana and van Winkle (1966) [79]	1	298.14	0.101325	0.07	-	-	-	-	0.07
Tardajos et al. (1986) [80]	1	298.14	0.101325	0.088	-	-	-	-	0.088
This Work	40	299 - 363	0.0 – 91.3	0.057	-	-	-	-	0.057
Tojo and Diaz (1995) [81]	1	298.15	0.101325	0.057	-	-	-	-	0.057
Torín-Ollarves et al. (2013) [35]	48	273 - 334	0.1 – 70.0	0.072	-	-	-	-	0.072
Treszczanowicz et al. (2010) [82]	1	298.15	0.101325	0.021	-	-	-	-	0.021
Treszczanowicz et al. (2010) [83]	1	298.15	0.101325	0.021	-	-	-	-	0.021
Vega-Maza et al. (2013) [34]	48	273 - 334	0.1 – 70.0	0.02	-	-	-	-	0.02
von Braun (1911) [84]	1	293.14	0.101325	0.86	-	-	-	-	0.86
Wang et al. (2004) [85]	1	298.15	0.101325	0.047	-	-	-	-	0.047
Weissler and Del Grosso (1950) [86]	2	293 - 304	0.101325	0.073	-	-	-	-	0.073
Wibaut and Geldof (1946) [87]	2	293 - 299	0.101325	0.068	-	-	-	-	0.068
Wilkinson (1931) [88]	1	293.14	0.101325	0.51	-	-	-	-	0.51
Wright (1960) [89]	1	273.15	0.101325	0.48	-	-	-	-	0.48
Yang et al. (2018) [90]	176	283 - 363	0.1 - 100	0.2	-	-	-	-	0.2
Zaripov et al. (2010) [91]	1	298.15	0.101325	0.78	-	-	-	-	0.78
Zotov et al. (1975) [92]	1	293.14	0.101325	0.026	-	-	-	-	0.026
Zotov et al. (1995) [30]	1	293.15	0.101325	0.029	-	-	-	-	0.029

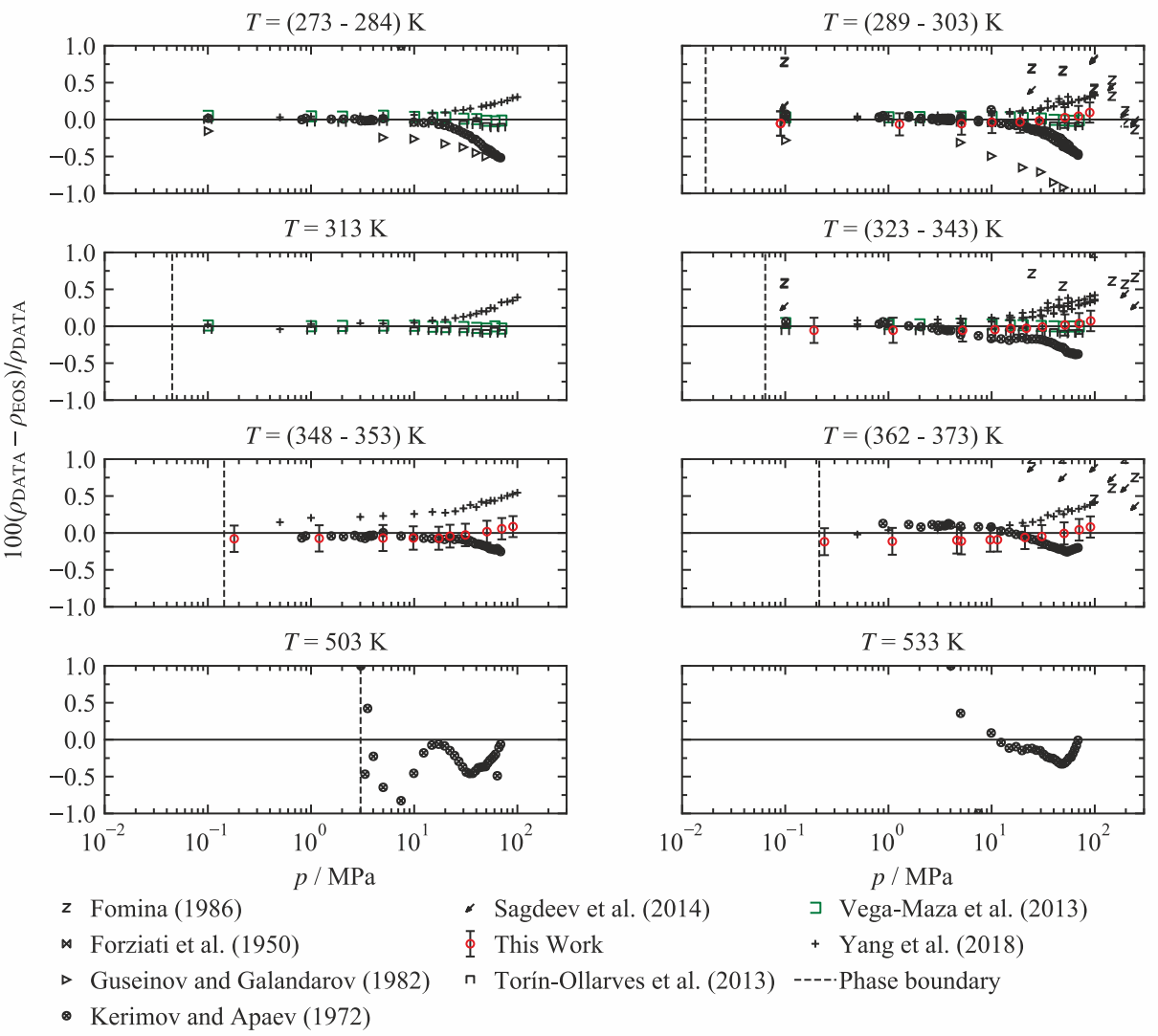

Figure 6. Percentage deviations of selected homogeneous density data from the present equation of state at selected isotherms.

Figure 6 illustrates percentage deviations of selected homogeneous density data from the equation of state. It reveals contradictory trends of the datasets of Kerimov and Apaev [58], Guseinov and Galandarov [55], and Yang et al. [90] to the already discussed datasets. Fairly good agreement between these datasets can be observed for most isotherms at pressures of up to approximately 10 MPa. Above 10 MPa, the deviations diverge. While deviations of Kerimov and Apaev [58] and Guseinov and Galandarov [55] show a trend in negative direction, the deviations of Yang et al. [90] exhibit a positive trend. Yang et al. [90] utilized an Anton Paar DMA HPM vibrating-tube densimeter for their density measurements, applying the same calibration method and reference fluids as Vega-Maza et al. [34] and Torín-Ollarves et al. [35]. Therefore, discrepancies between the datasets are probably not arising from the measurement principle or calibration method. Another error source may result from the sample purity. Yang et al. [90] used samples with a lower purity of 99 mass % and no further purification was done. Hence, contamination with e.g. water may explain the discrepancies. However, since no information about the composition of impurities is given, the influence of contaminations could not be reasonably investigated. The authors estimate the uncertainties for density and temperature to be 0.6 kg·m^{-3} and 16 mK (k = 2), respectively. The uncertainty of pressure is given as 0.062 MPa for $p \leq 60$ MPa and 0.192 MPa for 60 MPa < p < 140 MPa, which corresponds to relative expanded combined uncertainties between 0.081 % and 0.094 % (k = 2). The AARD of the dataset is 0.20 % with a maximum deviation of 0.39 %. Therefore, a reproduction within the experimental uncertainty was not achieved here. None of the data of Yang et al. [90] were fitted, since they are inconsistent at high pressures with the present measurements and the datasets of Vega-Maza et al. [34] and Torín-Ollarves et al. [35].

Kerimov and Apaev [58] provided the most comprehensive dataset, with 493 data points in the temperature range from 283 K to 533 K and pressures of up to 69 MPa. This publication is one of just two, which comprises data in the supercritical and critical region. Since the original publication could not be found in the literature, the data were taken from the Dortmund Data Bank [93] (DDB) for thermophysical properties. Information on the experimental uncertainty was not accessible to us. Nevertheless, since there were no other data available, they were used for fitting the critical and supercritical region with very little weight and keeping the same trend as observed in the lower temperature region. The equation of state represents the dataset of Kerimov and Apaev [58] in the liquid phase with an AARD of 0.27 %. In the supercritical region of medium- and high-density, the AARD is 0.75 % and 0.37 %, respectively. In the critical region, the data are represented with an AARD of 2.5 %. Deviations in the critical region were determined with regard to pressure deviations instead of density deviations, since small isothermal pressure changes cause large changes of density.

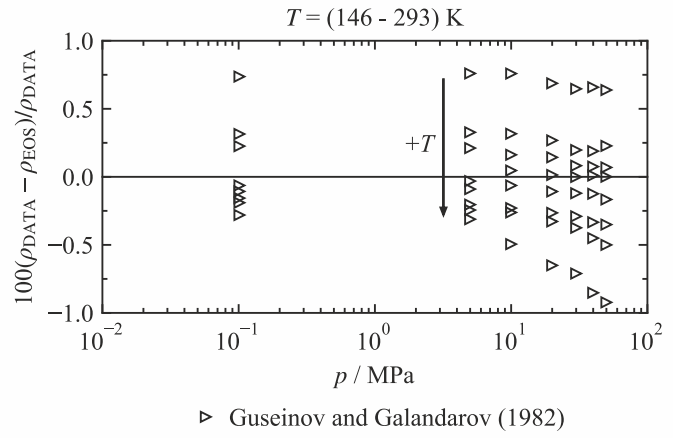

Figure 7. Percentage deviations of homogeneous density data of Guseinov and Galandarov [55] from the present equation of state.

For temperatures below 273 K, Guseinov and Galandarov [55] provided the most comprehensive dataset. 56 liquid density data points were measured with the hydrostatic weighing method at temperatures between 146 K and 294 K and pressures of up to 50 MPa. No detailed information about the measurement devices, sample handling and purity or uncertainty estimation are provided in that publication. Although the data seem consistent, they exhibit a trend towards negative deviations with increasing temperature and pressure (cf. Figure 7). Since no comparative data were available for temperatures below 273 K at elevated pressures, a direct validation was not possible. However, in overlapping state regions, the data exhibit quite large deviations of 0.5 % from those of Vega-Maza et al. [34]. The equation of state represents the dataset with an AARD of 0.30 % with a maximum deviation of 0.92 %.

The dataset of Fomina [50] extends the experimentally covered pressure range up to 245 MPa. The author reported 52 data points along seven isobars between ambient pressure and 245 MPa in the temperature range from 298 K to 472 K. The data scatter significantly and show a poor agreement with data from other publications. Since the original publication was not available to us, the data were taken from the DDB [93]. Information about the experimental uncertainty or sample purity was also not available. Due to the poor agreement with other measurements, these data were considered to be unreliable and were, therefore, not used for the development of the present equation of state. The dataset is reproduced with an AARD of 0.57 % and a maximum deviation of 1.6 %. The apparatus employed by Fomina [50] was later revised and re-designed by Sagdeev et al. [94] for simultaneous density and viscosity measurements. Sagdeev et al. [78] reproduced the measurements of Fomina [50] at 29 state points in the temperature range from 298 K to 472 K and pressures of up to 245 MPa. The two datasets deviate by 0.13 % to 0.77 % from each other. The scatter of the data of Sagdeev et al. [78] is less pronounced, which indicates better consistency. Sagdeev et al. [94] estimated the combined expanded uncertainty for the density of *n*-heptane to be 0.15 % to 0.3 % (k = 2), depending on temperature and pressure. This estimation was adapted by Sagdeev et al. [78] for 1-hexene. Similar to the data of Fomina [50], the dataset of Sagdeev et al. [78] seems to be inconsistent with the already discussed datasets, which might be due to the relatively low sample purity of 98 mol %. Therefore, this dataset was also considered to be unreliable and, thus, was not used for the development of the equation of state. The AARD is 0.54 % with a maximum deviation of 0.77 %.

Due to the strong discrepancies between the literature data in the higher-pressure range, we have carried out our own measurements in this work, cf. Sec. 3.2.1. These data extend the previously discussed datasets to slightly higher temperatures and pressures. Figure 6 illustrates that the present density data are represented within their experimental uncertainty of 0.18 % over the entire state region. The AARD is 0.057 % with a maximum deviation of 0.12 %. This confirms the selection of Vega-Maza et al. [34] and Torín-Ollarves et al. [35] as the basis for the development of the present equation of state.

The majority of the available experimental data at atmospheric pressure are represented within 0.1 %. Figure

8 illustrates percentage deviations of selected homogeneous density data measured at or close to atmospheric pressure. The most accurate data found in the literature are the ones of Forziati et al. [51]. The authors state the uncertainty in density to be 0.0001 g·ml^{-1} or less, which corresponds to a relative uncertainty of 0.03 % (k = 2). That dataset is reproduced with an AARD of 0.006 % and, thus, within the experimental uncertainty.

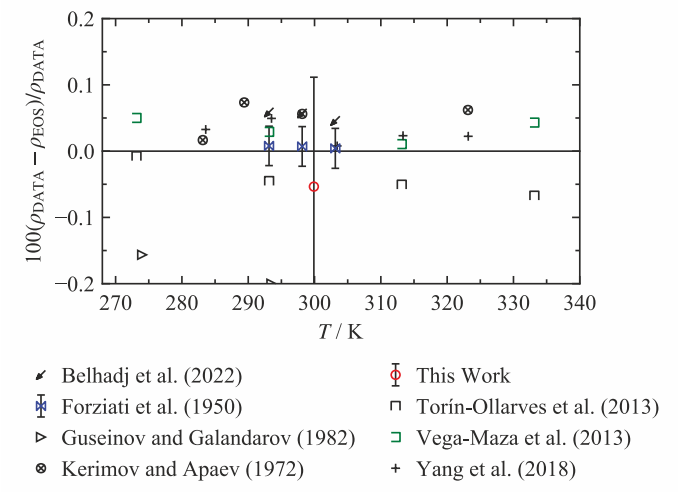

Figure 8. Percentage deviations of selected homogeneous density data from the present equation of state at atmospheric pressure.

In contrast to the homogeneous density, the database for saturated densities is limited to just two data sets of Kireev [95] and Ma et al. [27]. Kireev [95] measured 18 saturated liquid density data points at temperatures from 153 K to 474 K. The original publication was not found in the literature. Thus, the data were taken from the NIST ThermoData Engine [96] (TDE). Since no information regarding experimental uncertainty and sample purity were available to us, the reliability of this data could not be assessed. Nevertheless, the dataset is well reproduced with an AARD of 0.21 %. Ma et al. [27] reported 13 state points along the saturated liquid line and 4 state points along the saturated vapor line in the temperature range from 389 K to 500 K. Compared to the dataset of Kireev [95], the saturated liquid density data of Ma et al. [27] appear to be less consistent. The data scatter significantly and could only be reproduced with an overall AARD of 1.3 % and a maximum deviation of 2.5 % (cf. Figure 9). The saturated vapor densities deviate even more, with an AARD of 14 % and a maximum deviation of 24 %. Since no comparative data for saturated vapor densities were available and no detailed information about the accuracy of this data or sample purity could be obtained from this publication, the data could not be validated. However, due to the poor agreement of the saturated liquid density data to the dataset of Kireev [95], this dataset is considered to be unreliable.

Owing to the limited database of saturated densities, the phase boundary was defined by fitting homogeneous liquid density data in the vicinity to the phase boundary and vapor pressure data (cf. Sec. 5.2) as well as by applying constraints for the course of the rectilinear diameter (cf. Sec. 6).

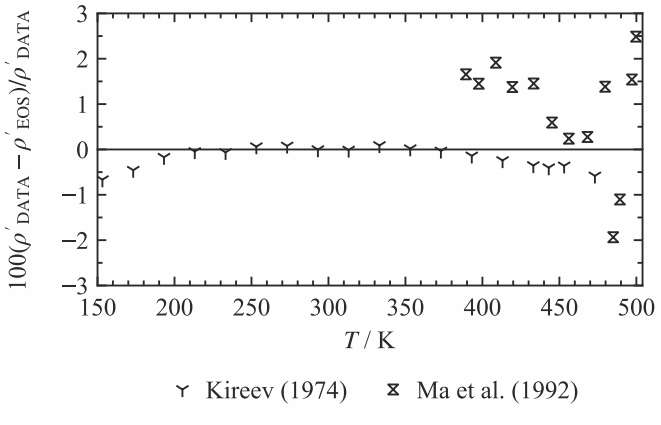

Figure 9. Percentage deviations of saturated liquid density data from the present equation of state.

Table 13: Average absolute relative deviations (AARD) of saturated density data from the present equation of state.

			AARD / %			
Reference	N	$(T_{min} - T_{max})$ / K	LT	MT	HT	Overall
Saturated liquid density ρ'						
Kireev [95]	18	153 – 474	0.19	0.22	-	0.21
Ma et al. [27]	13	389 - 500	-	1.2	2.0	1.3
Saturated vapor density ρ''						
Ma et al. [27]	4	484 -500	-	7.5	21	14

The uncertainty of density data calculated with the present equation of state is estimated based on the representation of the available datasets and their corresponding experimental uncertainties. Since no homogeneous vapor phase data were available in the literature and the data in the critical and supercritical region lack realistic uncertainty estimations, only uncertainties for densities in the liquid phase can be defined. The uncertainty of liquid density data at atmospheric pressure and temperatures between 270 K and 340 K is estimated to be 0.1 %. The measurements of Forziati et al. [51] indicate that the actual uncertainty might be smaller. However, for a reliable statement, more comprehensive measurements are required. For the temperature range between 273 K and 333 K for pressures of up to 70 MPa, the uncertainty of the present equation of state is 0.1 %, based on data of Vega-Maza et al. [34]. For pressures of up to 95 MPa and temperatures of up to 360 K,

the uncertainty increases to 0.18 % based on the present measurements.

5.2. Vapor pressure

The data base for the vapor pressure consists of 247 data points, compiled from 69 publications. In Table 14, the corresponding publications are listed, together with the covered temperature range and the AARD. Overall, the investigated temperature ranges from 215 K up to the critical temperature. However, the majority of the data was measured in a limited temperature range from 275 K to 378 K. Figure 10 illustrates percentage deviations of selected datasets.

Forziati et al. [51] measured the vapor pressure at 14 different state points in the temperature range between 289 K and 338 K at apparatus-specific fixed pressures. These fixed pressures were previously calibrated, by measuring the temperature of water under vapor-liquid equilibrium. The corresponding pressures were taken from Osborne and Meyer [97]. The purity of the sample is given as 99.86 mol %. To avoid contamination, the sample was introduced in the apparatus without contact with air. The authors did not report any experimental uncertainties. However, the measurements were carried out at the National Bureau of Standards and are therefore considered to be reliable. In addition, the density data from the same publication (cf. Sec. 5.1) were highly consistent. To assess the quality of the data, the uncertainty was estimated in this work. The temperature was measured utilizing a platinum resistance thermometer (25 Ω). Therefore, the uncertainty of temperature was conservatively estimated to be 0.05 K (k = 1.73). The uncertainty of pressure was assumed to be the maximum difference between the vapor pressure data of water according to Osborne and Meyers and the IAPWS-95 by Wagner and Pruß [17]. In the corresponding pressure range, the difference does not exceed 6.9 Pa. Hence, the uncertainty of pressure was assumed to be 6.9 Pa (k = 1.73). Applying Gaussian error propagation, the expanded combined uncertainty is less than 0.12 % (k = 2). One data point was fitted so that the entire dataset is represented with an AARD of 0.056 % and a maximum deviation of 0.12 %.

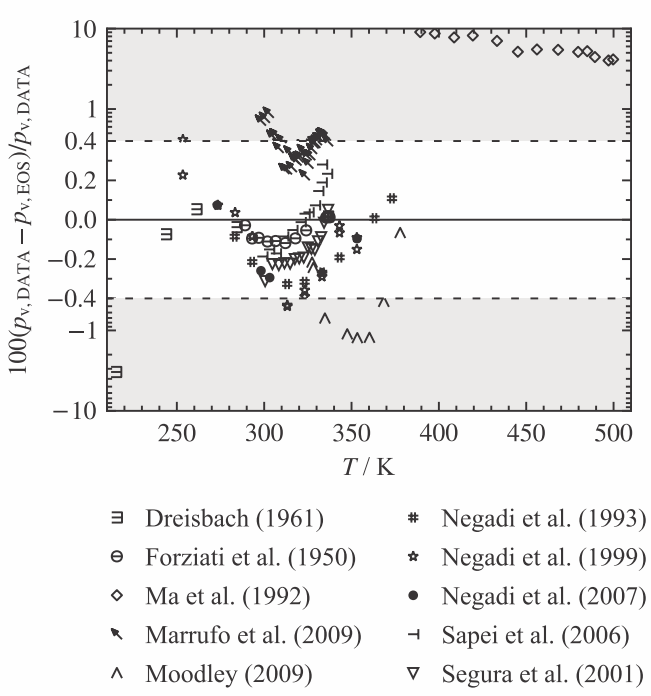

Figure 10. Percentage deviations of selected vapor pressure data from the present equation of state. The ordinate is linearly scaled between the dashed lines and logarithmically scaled in the gray shaded regions.

Several measurements of the vapor pressure of 1-hexene were published by Negadi and co-workers [98–100]. The data cover a temperature range from 253 K to 373 K. Negadi et al. [99] stated uncertainties for pressure and temperature of 0.3 % and 0.02 K (k = 1), respectively. The temperature stability is given as 0.01 K. The corresponding calculated expanded combined uncertainties are 0.63 % (k = 2) on average. Additional measurements were carried out by Negadi et al. [100] at temperatures between 273 K and 353 K with an updated temperature and pressure measurement chain. The authors stated slightly lower uncertainties of 0.2 % and 0.01 K (k = 1) for pressure and temperature, respectively. This results in combined expanded uncertainties of less than 0.49 % (k = 2). The samples used by Negadi et al. [98,99] were obtained from Janssen Chimica (Belgium) with a stated purity of 97 mol % and used without further purification. Negadi et al. [100] obtained their sample from the same supplier, but determined the purity prior to the measurements to 99 mol % via gas liquid chromatography. Since the three datasets agree remarkably well, the purity of the samples used by Negadi et al. [98,99] is assumed to be the same. By adjusting the equation of state to two data points of Negadi et al. [98], both datasets of Negadi et al. [98,99] can be reproduced with deviations of less than 0.32 % and 0.50 %, respectively. The data of Negadi et al. [100] are represented within 0.33 %. Thus, all datasets are reproduced within their

experimental uncertainties. These data are confirmed by the datasets of Sapei et al. [101] and Segura et al. [102], which are reproduced with AARD of 0.13 % and 0.17 %, respectively.

To expand the validity of the equation of state to lower temperatures, two vapor pressure data of Dreisbach [23] were fitted at 243.87 K and 284.25 K, which also led to a better representation of low-temperature data of Negadi et al. [98–100]. Due to the good agreement with experimental data of other publications [51,98–100,102], this dataset is considered to be reliable, although no uncertainties are stated. The AARD of 0.65 % is very high, which is caused by the deviation (3.3 %) of the data point at 215 K. Since no comparative data were available for temperatures below 243 K, this data point could not be validated.

Beyond 378 K up to the critical temperature, only Ma et al. [27] reported vapor pressure data. Similar to the saturation density data (cf. Sec. 5.1), their vapor pressure data are of disputable quality. No detailed information about the uncertainty of this data could be obtained from this publication. The dataset is reproduced with an AARD of 6.1 % and a maximum deviation of 9 %.

Based on the experimental data, the uncertainty of the vapor pressure calculated with the present equation of state is estimated to be 0.5 % in the temperature range from 273 K to 363 K. Outside of this region, no reliable statement can be made.

To validate the performance with respect to the vapor pressure, the equation of state was compared to experimental data of the enthalpy of vaporization data. Vapor pressure and enthalpy of vaporization are related according to Eq. (21)

$$\frac{\mathrm{d}p_\mathrm{v}}{\mathrm{d}T} = \frac{h_\mathrm{vap}}{T(v'' - v')}, \tag{21}$$

where v'' and v' are the molar volume of the saturated vapor and saturated liquid phase, respectively. However, the database is limited to four data points from two publications by Camin et al. [103] and Lide and Kehiaian [29]. Both reported data at 298 K and 336 K. None of the data points was fitted. Nevertheless, the datasets are reproduced with an AARD of 0.074 % and 0.096 %, respectively. Even though the comparison is of limited significance due to the small number of data points, the low deviations indicate a reasonable behavior and good performance of the equation of state.

Table 14: Average absolute relative deviations (AARD) of vapor pressure data from the present equation of state.

			AARD / %			
Reference	N	$(T_\mathrm{min} - T_\mathrm{max})$ / K	LT	MT	HT	Overall
Alonso-Tristán et al. (2008) [104]	4	313 - 314	-	0.4	-	0.4
Ambrose et al. (1974) [105]	1	336.58	-	0.098	-	0.098
Belabbaci et al. (2014) [106]	3	313 - 314	-	0.34	-	0.34
Belabbaci et al. (2015) [107]	4	313 - 314	-	0.29	-	0.29
Bourguel (1927) [41]	1	337.87	-	4	-	4
Budantseva et al. (1973) [108]	1	336.43	-	0.57	-	0.57
Campbell and Eby (1941) [44]	2	336 - 337	-	1.5	-	1.5
Campbell and O'Connor (1939) [45]	1	336.12	-	0.85	-	0.85
Chamorro et al. (1999) [109]	3	313 - 314	-	0.43	-	0.43
Chamorro et al. (2002) [110]	4	313 - 314	-	0.33	-	0.33
Chamorro et al. (2004) [111]	2	313 - 314	-	0.39	-	0.39
Desty and Fidler (1951) [48]	1	336.62	-	0.031	-	0.031
Dojčanský et al. (1967) [49]	1	298.14	0.62	0	-	0.62
Dreisbach (1961) [23]	5	215 - 337	0.81	0.017	-	0.65
Fischer and Gmehling (1996) [112]	2	347 - 364	-	0.99	-	0.99
Forziati et al. (1950) [51]	14	289 - 338	0.082	0.046	-	0.056
Geiseler and Pilz (1962) [54]	1	336.87	-	0.82	-	0.82
Ghellai et al. (2013) [113]	3	313 - 314	-	0.34	-	0.34
Gmehling (1983) [114]	2	323 - 334	-	0.48	-	0.48
Hani et al. (2012) [115]	8	263 - 334	0.52	0.68	-	0.6
Hanson and van Winkle (1967) [116]	1	333.12	-	0.01	-	0.01
Herz (1916) [21]	1	339.97	-	11	-	11
Hirawan et al. (2014) [117]	3	313 - 364	-	0.16	-	0.16
Hollenshead and Van Winkle (1966) [56]	1	336.52	-	0.29	-	0.29
Humphrey and Van Winkle (1967) [118]	1	336.63	-	0.062	-	0.062
Jabloniec et al. (2007) [119]	2	302 - 364	-	0.88	-	0.88
Jackowski (1985) [120]	1	298.16	0.37	0	-	0.37
Jonasson et al. (1994) [121]	2	315 - 334	-	4.1	-	4.1
Kirss et al. (1975) [122]	1	328.14	-	0.095	-	0.095

Reference	N	$(T_{min} - T_{max})$ / K	AARD / %			
			LT	MT	HT	Overall
Koch and van Raay (1954) [123]	1	336.62	-	0.031	-	0.031
Krollpfeiffer and Seebaum (1928) [59]	2	336 - 338	-	1.5	-	1.5
Kudryavtseva et al. (1968) [60]	4	301 - 337	5.1	0.43	-	1.6
Kudryavtseva et al. (1969) [61]	1	336.63	-	0.06	-	0.06
Lesteva et al. (1985) [124]	1	336.63	-	0.06	-	0.06
Letcher et al. (2004) [125]	2	278 - 299	0.093	0	-	0.093
Lide and Kehiaian (1994) [29]	2	298 - 337	0.18	0.059	-	0.12
Lozano et al. (1997) [126]	2	313 - 314	-	0.28	-	0.28
Ma et al. (1992) [27]	13	389 - 505	-	6.5	4.1	6.1
Marrufo et al. (2009) [69]	31	298 - 337	0.75	0.39	-	0.41
Mears et al. (1950) [71]	1	336.61	-	0.001	-	0.001
Melikhov et al. (1991) [72]	1	336.65	-	0.11	-	0.11
Moodley (2009) [127]	8	327 - 378	-	0.66	-	0.66
Negadi et al. (1993) [98]	8	283 - 374	0.15	0.2	-	0.19
Negadi et al. (1999) [99]	15	253 - 354	0.17	0.26	-	0.23
Negadi et al. (2007) [100]	11	273 - 364	0.16	0.21	-	0.19
Ogorodnikov et al. (1961) [74]	1	336.72	-	0.35	-	0.35
Pukinskii et al. (1982) [76]	1	336.8	-	0.59	-	0.59
Reid et al. (1987) [25]	1	336.61	-	0.003	-	0.003
Renon and Prausnitz (1968) [77]	1	333.12	-	0.098	-	0.098
Sapei et al. (2006) [101]	13	298 - 337	0.19	0.12	-	0.13
Sapei et al. (2007) [128]	2	323 - 334	-	0.11	-	0.11
Segovia (1997) [129]	10	313 - 314	-	0.33	-	0.33
Segovia et al. (1998) [130]	3	313 - 314	-	0.3	-	0.3
Segura et al. (2001) [102]	15	300 - 337	0.31	0.16	-	0.17
Suryanarayana and Van Winkle (1966) [79]	1	336.62	-	0.031	-	0.031
Tassios and Van Winkle (1967) [131]	1	353.12	-	0.53	-	0.53
Timmermans (1927) [132]	1	336.47	-	0.44	-	0.44
Vera and Prausnitz (1971) [133]	3	283 - 324	0.082	0.075	-	0.078
Villamañán et al. (2008) [134]	3	313 - 314	-	0.38	-	0.38
Villamañán et al. (2009) [135]	2	313 - 314	-	0.4	-	0.4
von Braun (1911) [84]	1	335.62	-	0.48	-	0.48
von Braun et al. (1929) [136]	1	340.62	-	13	-	13
Wentink et al. (2005) [137]	1	336.5	-	0.36	-	0.36
Wilkinson (1931) [88]	1	335.12	-	4.6	-	4.6
Wisniak and Gabai (1996) [138]	1	336.65	-	0.14	-	0.14
Wright (1960) [89]	1	337.22	-	1.9	-	1.9
Yañez Torres et al. (1992) [139]	2	328 - 339	-	0.13	-	0.13
Zotov et al. (1975) [92]	1	336.73	-	0.38	-	0.38
Zotov et al. (1995) [30]	1	336.75	-	0.43	-	0.43

5.3. Speed of sound

The speed of sound database comprises 315 data points, including the measurements presented in Secs. 3.2.2 and 3.2.3 and literature data taken from eleven publications. Therefore, it is the most comprehensive database for caloric properties. Most of the data were measured in the homogeneous liquid phase at temperatures between 215 K and 500 K and pressures of up to 151 MPa. Additionally, one dataset for the saturated liquid phase between 153 K and 493 K was available. In Table 15, the AARD of every dataset is given, together with the experimentally covered temperature and pressure range. Figure 11 illustrates the percentage deviations between the equation of state and all available datasets.

For the development of the equation of state, the data obtained from apparatus 1 (cf. Sec. 3.2.2) were fitted. This dataset was found to be highly consistent and is well represented with an AARD of 0.024 % and a maximum deviation of 0.08 %, and, thus within the experimental uncertainty of 0.15 %. Furthermore, the data show a good agreement with the measurements carried out with apparatus 2 and the dataset of Khasanshin et al. [140] in overlapping state regions (cf. Figure 12). Khasanshin et al. [140] reported 73 speed of sound data points, measured with the pulse-echo overlap method along eight isotherms between 303 K and 433 K and pressures of up to 100 MPa. Standard uncertainties of temperature, pressure, and speed of sound are given as 0.02 K, 0.05 %, and 0.1 % (k = 1), respectively, which yields an expanded combined uncertainty of 0.2 % (k = 2). The purity of the sample was stated as 99 mass % at least, and the sample composition was assessed prior to and after the measurements via gas-liquid chromatography, which revealed no change in composition. As a consequence, the measurements were highly reproducible within 0.03 %. Therefore, the equation

of state was fitted to data of Khasanshin et al. [140] for the extended temperature and pressure ranges of up to 433 K and 100 MPa, respectively. The dataset is reproduced with an AARD of 0.042 % and a maximum deviation of 0.17 % and, thus, within the experimental uncertainty.

Outside of the temperature range covered by Khasanshin et al. ,[140], data measured with apparatus 2 (cf. Sec. 3.2.3) were used for the development of the present equation of state.

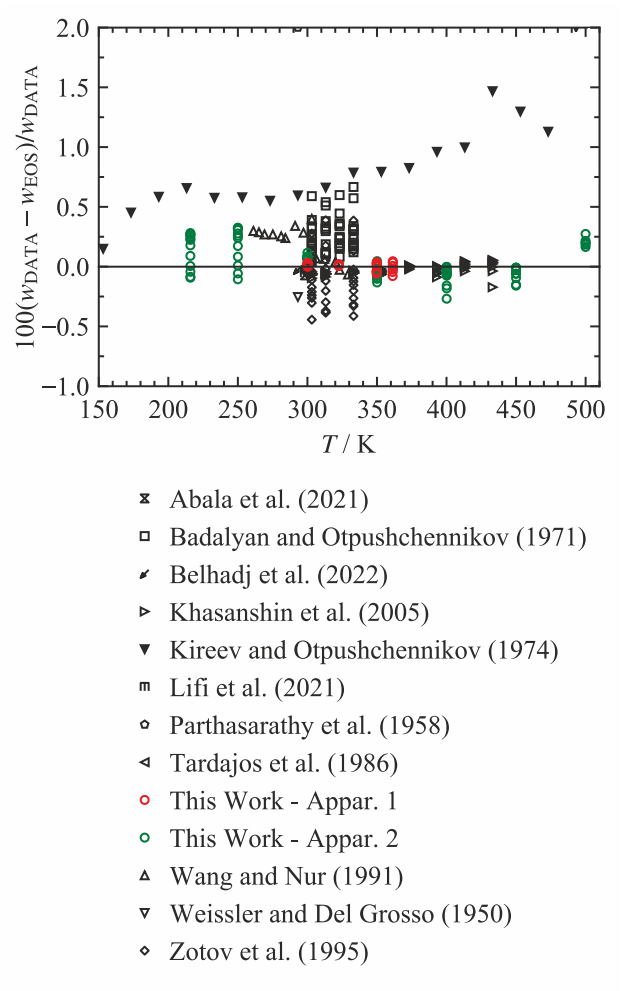

Figure 11. Percentage deviations of experimental speed of sound data from the present equation of state.

With these measurements, the database for the speed of sound was considerably extended to a temperature range from 215 K to 500 K for pressures of up to 151 MPa. The data are in good agreement with the previously discussed datasets and, thus, considered to be reliable. However, a representation within the experimental uncertainty was mostly not achieved. Although the data of the 215 K and 250 K isotherms appear very consistent, it was not possible to represent these data with deviations better than 0.2 %. No other publications report liquid phase data below 293 K so that a validation was not possible. Furthermore, fitting of these data with higher weights interfered with the representation of other experimental low-temperature data, especially heat capacities. The data for the high-temperature isotherms (400 K ≤ T ≤ 500 K) scatter around the present equation of state. The speed of sound varies significantly with small changes of temperature or pressure close to the phase boundary and the critical point. It could not be determined if there was an error in our measurements or our equation of state. Hence, the equation of state was not fitted to high temperature data above 400 K and it was not possible to represent the corresponding data within the experimental uncertainty.

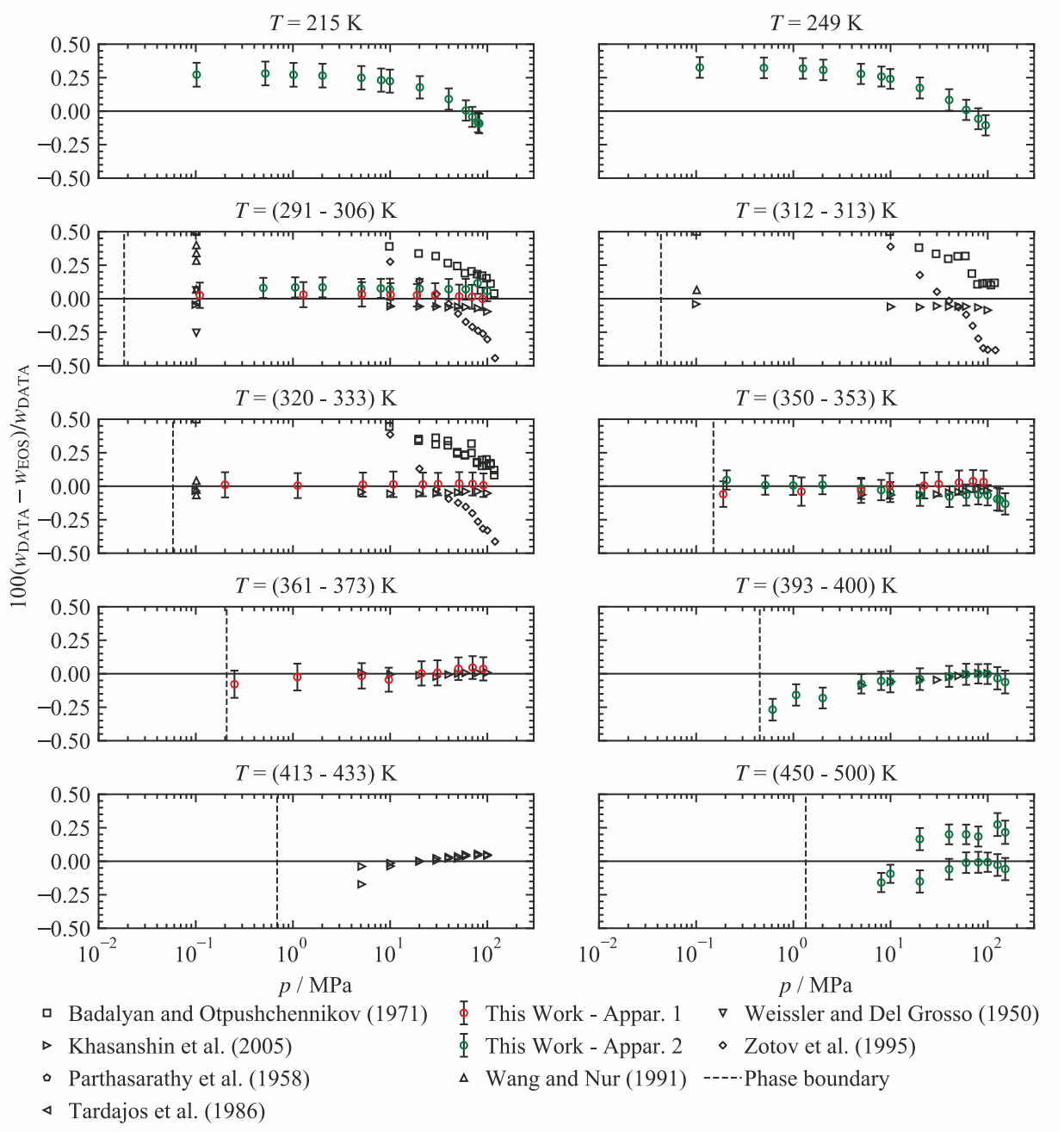

Figure 12. Percentage deviations of selected homogeneous speed of sound data from the present equation of state at selected isotherms.

The datasets of Badalyan and Otpushchennikov [141] and Zotov et al. [30] contain 52 and 34 data points, respectively, for temperatures between 303 K and 334 K and pressures below 121 MPa. The experimental uncertainty was claimed to be 0.2 % by Badalyan and Otpushchennikov [141] and between 0.35 % and 0.6 % by Zotov et al. [30]. Therefore, these datasets neither provide a comprehensive nor a qualitative expansion of the experimentally covered state region. Thus, they are not discussed further here.

Kireev and Otpushchennikov [142] provided the only speed of sound data measured in the liquid phase under vapor-liquid equilibrium. The original publication was not found in the literature. Thus, 18 datapoints were taken from the DDB [93]. The data are not consistent with the dataset of Khasanshin et al. [140] and the measurements carried out in this work. Therefore, relatively low weights were applied to avoid a deterioration of the representation of other speed of sound data. The dataset is represented with an AARD of 0.99 % and a maximum deviation of 4.7 % in the vicinity of the critical point.

Based on the representation of the experimental data, provided in Sec. 3.2.2 and Khasanshin et al. [140], the

uncertainty of calculated speed of sound data is estimated to be 0.15 % in the temperature range from 300 K to 362 K for pressures of up to 90 MPa and 0.2 % for higher pressures of up to 100 MPa and temperatures of up to 433 K.

Table 15: Average absolute relative deviations (AARD) of speed of sound data from the present equation of state.

				AARD / %					
Reference	N	$(T_{min} - T_{max})$ / K	$(p_{min} - p_{max})$ / MPa	liq.	crit.	LD	MD	HD	Overall
Abala et al. (2021) [38]	1	298.15	0.1	0.073	-	-	-	-	0.073
Badalyan and Otpushchennikov (1971) [141]	52	303 - 334	0.1 - 118	0.27	-	-	-	-	0.27
Belhadj et al. (2022) [40]	3	293 – 304	0.1	0.019	-	-	-	-	0.019
Khasanshin et al. (2005) [140]	73	303 - 434	0.1 - 101	0.042	-	-	-	-	0.042
Lifi et al. (2021) [68]	1	298.15	0.1	0.054	-	-	-	-	0.054
Kireev and Otpushchennikov (1972) [142]	18	153 - 494	<0.1 – 2.7	0.99	-	-	-	-	0.99[a]
Parthasarathy et al. (1958) [143]	1	293.14	0.101325	2.1	-	-	-	-	2.1
Tardajos et al. (1986) [144]	1	298.14	0.101325	0.033	-	-	-	-	0.033
This Work - Appar. 1	36	300 - 362	0.1 – 91.3	0.024	-	-	-	-	0.024
This Work - Appar. 2	79	215 - 500	0.1 - 151	0.12	-	-	-	-	0.12
Wang and Nur (1991) [145]	14	261 - 330	0.101325	0.21	-	-	-	-	0.21
Weissler and Del Grosso (1950) [86]	2	293 - 304	0.101325	0.16	-	-	-	-	0.16
Zotov et al. (1995) [30]	34	303 - 334	10.0 - 121	0.22	-	-	-	-	0.22

[a]dataset contains data in the saturated liquid phase only

5.4. Isobaric Heat Capacity and Saturation Heat Capacity

For the isobaric heat capacity, 86 data points from six publications were available. All of these data were measured in the homogeneous liquid phase. They cover a temperature range from 186 K to 363 K and pressures of up to 196 MPa. In addition, 23 saturation heat capacities for the temperature range between 136 K and 308 K were provided by McCullough et al. [7]. Isobaric heat capacity and saturation heat capacity can be converted according to Eq. (22), as stated by Zábranský and Růžička [146]:

$$c_\sigma - c_p = -T\left(\frac{\partial v}{\partial T}\right)_p \left(\frac{\mathrm{d}p}{\mathrm{d}T}\right)_{\mathrm{sat}}, \qquad (22)$$

where c_p is the isobaric heat capacity and c_σ is the saturation heat capacity. However, the difference is negligible outside of the vicinity of the critical region so that the data of McCullough et al. [7] were directly compared to c_p data. The AARD of all datasets is listed in Table 16 and percentage deviations from the equation of state are illustrated in Figure 13.

For the adjustment of the equation of state to heat capacity data, the datasets of Kalinowska and Wóycicki [147] and McCullough et al. [7] were of main interest. Both research groups are considered to have a high level of expertise in the measurement of caloric properties. Sabbah et al. [148] recommend reference values for heat capacities of naphthalene and *n*-heptane, including data of McCullough et al. [149] and Douglas et al. [150], respectively. Sabbah et al. [148] highlight the excellent agreement of the datasets for *n*-heptane between Douglas et al. [150] and Kalinowska et al. [151]. Kalinowska and Wóycicki [147] measured isobaric heat capacities with an adiabatic calorimeter in the temperature range from 186 K to 301 K at ambient pressure. The sample was degassed via distillation under reduced pressure and the purity was estimated to be 99.72 mol %. The authors did not report any uncertainties. McCullough et al. [7] also utilized an adiabatic calorimeter. The authors stated the purity of their sample to be between 99.95 mol % and 99.97 mol %. It was dried with calcium hydride and filled into the calorimeter via vacuum distillation, to avoid any further contamination. The uncertainty was claimed to be 0.2 %. However, it was not specified, whether this is a standard or combined uncertainty. Both datasets seem to be consistent with other properties, such as speed of sound or density. However, fitting of both datasets simultaneously did not lead to a stable form of the equation of state. Due to the better documentation of the measurement procedure, uncertainty estimation, higher purity and additional drying of the sample, the data of McCullough et al. [7] were considered to be more reliable and the equation of state was fitted to these data. The complete dataset is represented within 0.11 % and, thus, within the indicated uncertainty.

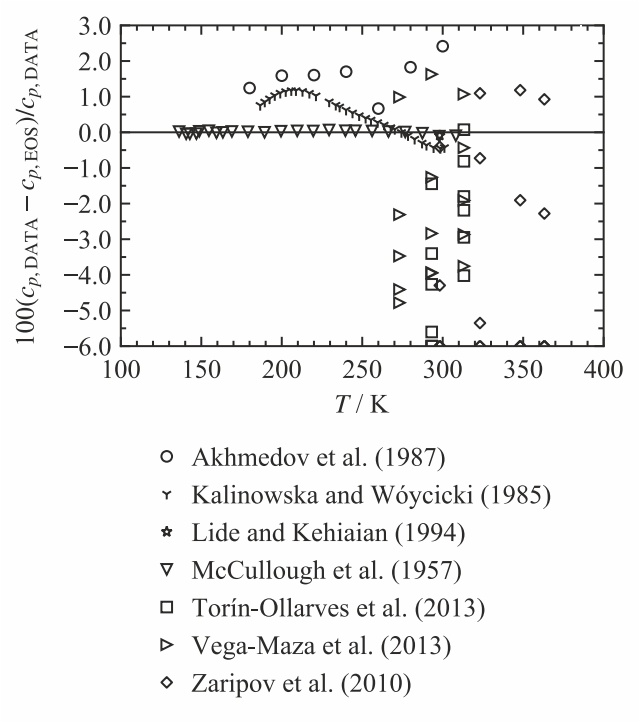

Figure 13. Percentage deviations of isobaric heat capacity data in the liquid phase from the present equation of state. Data of McCullough et al. [7] are saturation heat capacities.

Experimental isobaric heat capacities at elevated pressures can be found in the publications of Vega-Maza et al. [34], Torín-Ollarves et al. [35], and Zaripov et al. [91]. Vega-Maza et al. [34] performed measurements with a nonadiabatic flow calorimeter in the temperature range from 273 K to 313 K for pressures of up to 20 MPa. Torín-Ollarves et al. [35] reproduced the data with the same apparatus for the 293 K and 313 K isotherms and extended the pressure range up to 25 MPa. Applying the Gaussian error propagation law to the stated standard uncertainties for temperature, pressure, and isobaric heat capacity, the expanded combined uncertainty yields 0.6 % (k = 2) for both datasets. This uncertainty estimation seems to be too optimistic, since the data of Vega-Maza et al. [34] for the 293 K isotherm were reproduced by Torín-Ollarves et al. [35] with deviations significantly larger than 0.6 %. Zaripov et al. [91] expanded the covered temperature and pressure range with isobaric heat capacity data up to 363 K and 196 MPa. The authors estimated their uncertainty to be 2 % (k = 2). However, it was not possible to adjust the equation of state to any high-pressure data without deterioration of the speed of sound data. The relative deviation between the equation of state and experimental isobaric heat capacity data of Vega-Maza et al. [34] and Torín-Ollarves et al. [35] are approximately 2.6 % and 3.4 %, respectively. The data of Zaripov et al. [91] deviate by 6.6 % on average and even exceed 15 % at the highest pressures. Thus, the representation of experimental heat capacities at high pressures within their experimental uncertainties was not achieved. An estimation of the uncertainty of the equation of state for the isobaric heat capacity was not possible due to the lack of reliable data. However, the uncertainty of the saturation heat capacity of the saturated liquid phase and temperatures between 136 K and 308 K is estimated to be 0.2 % (k = 2) based on the measurements of McCullough et al. [7].

Table 16: Average absolute relative deviations (AARD) of isobaric heat capacity data from the present equation of state.

				AARD					
Reference	N	$(T_{\min} - T_{\max})$ / K	$(p_{\min} - p_{\max})$ / MPa	liq.	crit.	LD	MD	HD	Overall
Akhmedov et al. (1987) [152]	7	180 - 300	0.101325	1.6	-	-	-	-	1.6
Kalinowska and Wóycicki (1985) [147]	31	186 - 302	0.101325	0.62	-	-	-	-	0.62
Lide and Kehiaian (1994) [29]	1	298.15	0.101325	0.087	-	-	-	-	0.087
McCullough et al. (1957) [7]	23	136 - 309	<0.1 – 3.8E^{-2}	0.036	-	-	-	-	0.036 [a]
Torín-Ollarves et al. (2013) [35]	12	293 - 314	0.1 – 25.0	3.4	-	-	-	-	3.4
Vega-Maza et al. (2013) [34]	15	273 - 314	0.1 – 21.0	2.6	-	-	-	-	2.6
Zaripov et al. (2010) [91]	20	298 - 364	0.1 - 196	6.6	-	-	-	-	6.6

[a] dataset contains saturation heat capacities only

6. Extrapolation and Physical Behavior

In the previous sections, the representation of the experimental data with the present equation of state was discussed. However, experimental data for 1-hexene are predominantly available in the liquid phase and only to a limited extent in the gas phase and supercritical region. To validate the equation of state in regions, which are not covered by experimental data, the physical behavior was evaluated and analysed using different characteristic thermodynamic properties.

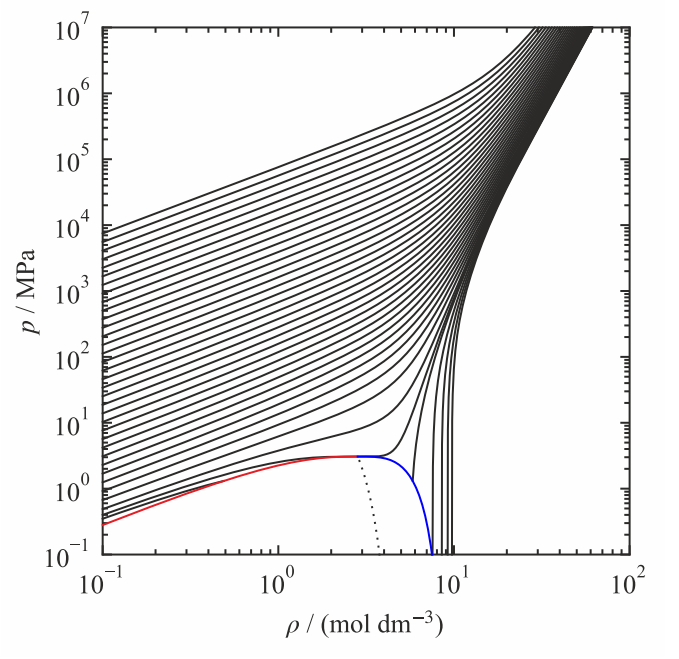

Figure 14. Double-logarithmic p,ρ-diagram showing the saturated liquid line (blue), saturated vapor line (red), isotherms (T_{max} = 10^7 K, black), and the rectilinear diameter ρ_{RD} (dashed line).

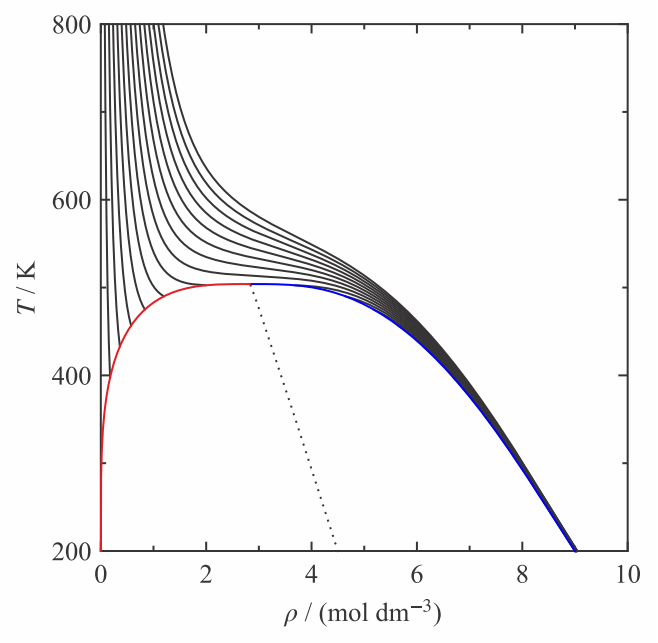

Figure 15. T,ρ-diagram showing the the saturated liquid line (blue), saturated vapor line (red), isobars (p_{max} = 7 MPa), and the rectilinear diameter ρ_{RD} (dashed line).

Thermal properties are illustrated in Figures 14 and 15. The slope and curvature of the critical isotherm are zero at the critical point, as shown in the double-logarithmic p,ρ-diagram (cf. Figure 14). All isotherms converge at high densities and pressures, without intersecting. The same behavior can be observed for the isobars in the T,ρ-diagram (cf. Figure 15), converging at high densities and temperatures. Furthermore, the rectilinear diameter $\rho_{RD} = (\rho' + \rho'') / 2$ appears as a straight line between the saturation lines in the T,ρ-diagram, which is consistent with an empirical correlation according to Cailletet and Mathias [153], after which the rectilinear diameter can be formulated as a linear function of temperature.

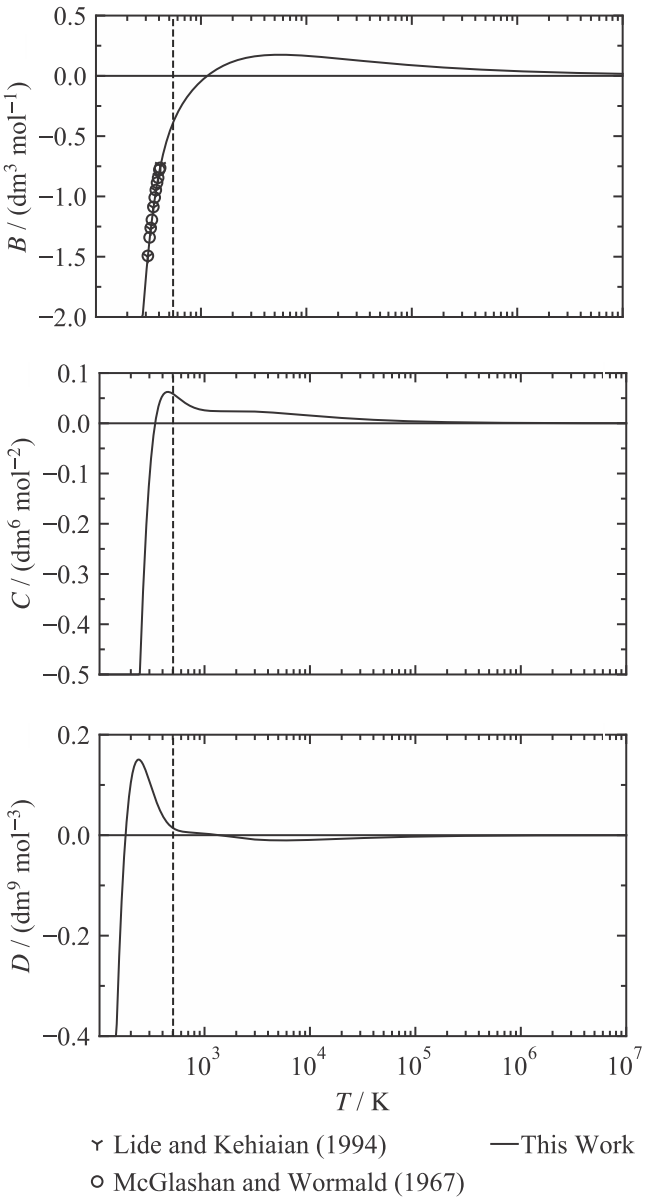

Figure 16. Second (B; top), third (C; middle), and fourth (D; bottom) thermal virial coefficients as a function of temperature. The dashed lines highlight the critical temperature T_c.

The representation of the second B, third C, and fourth D thermal virial coefficients confirms an adequate extrapolation behavior. Figure 16 depicts the coefficients as a function of temperature. At low temperatures, all three coefficients have positive slopes and negative curvatures, exhibit a global maximum, and asymptotically approach zero with increasing temperature. The maxima of C and D are slightly below the critical temperature. This behavior is

consistent with studies carried out by Thol et al. [154] for the Lennard-Jones fluid. For the second virial coefficient, literature data of Lide and Kehiaian [29] and McGlashan and Wormald [155] at temperatures between 313 K and 413 K are available. Both datasets show a good agreement with the equation of state; relative deviations are 0.7 % and 0.9 %, respectively.

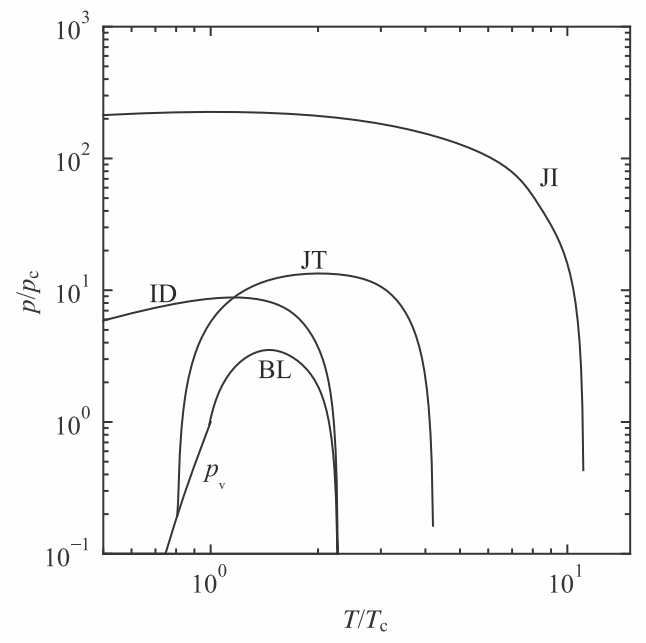

Figure 17. Vapor pressure p_v and ideal curves for the compressibility factor Z, calculated from the equation of state: Boyle curve (BL); ideal curve (ID); Joule-Thomson inversion curve (JT); Joule inversion curve (JI).

Nevertheless, deficiencies regarding the representation of C and D had to be accepted. In contrast to Thol et al. [154], the third viral coefficient does not show an inflection point, but a second weakly pronounced maximum. Furthermore, the fourth virial coefficient is slightly negative at high temperatures. Since the present equation of state is not of reference quality due to the limited underlying experimental database, these small deficiencies had to be accepted for a better representation of the experimental data. However, the ideal curves formulated in terms of the compressibility factor Z (cf. Figure 17) also confirm a reasonable extrapolation behavior. Since Z and the virial coefficients are directly linked via the virial expansion, B, C, and D determine the shape of the ideal curves. According to Span and Wagner [156], a visual assessment of the ideal curves is suitable for the evaluation of the extrapolation behavior of empirical equations of state. All curves show a negative curvature over the entire temperature and pressure range, without any bumps, discontinuities, or "overhanging". Hence, small shortcomings regarding the representation of C and D are assumed to be acceptable.

Figure 18 shows the residual isochoric heat capacity c_v^r as a function of temperature. Physically correct behavior is confirmed by the course of the saturation lines. They exhibit positive curvatures over the entire temperature range, intersect once and converge in a distinct maximum at the critical point. Additionally, the saturated vapor curve has a positive slope over the entire temperature range. Theoretically, the residual isochoric heat capacity is supposed to become infinite at the critical point. However, such a behavior cannot be modelled with analytical equations, but has to be approximated by means of Gaussian bell-shaped terms to impose a distinct peak at the critical point. The isobars should converge to small values at high temperatures to achieve a correct transition to the ideal gas. This requirement is also fulfilled by the present equation of state.

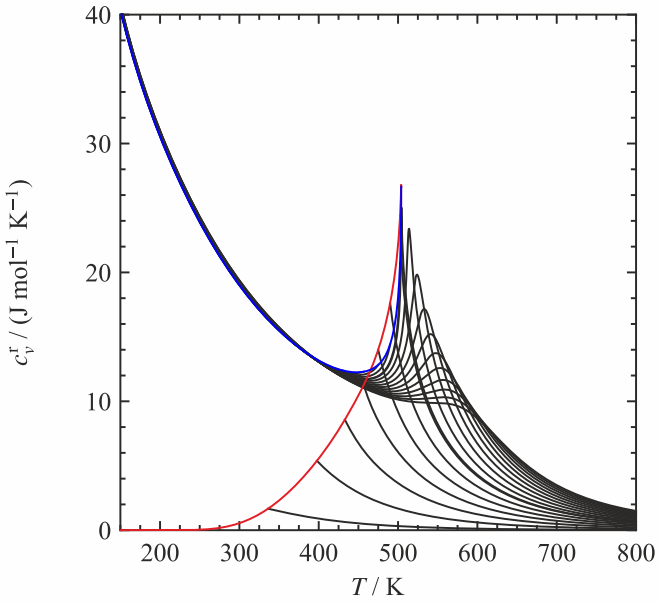

Figure 18. Residual isochoric heat capacity c_v^r as a function of temperature along the saturated liquid line (blue), saturated vapor line (red), and isobars (black).

Figure 19 shows the speed of sound as a function of temperature along the saturation lines and selected isobars. At the same pressure, the speed of sound in the liquid phase must be larger than in the vapor phase. The saturated vapor line should exhibit a negative curvature over the entire temperature range. Both saturation lines converge at the critical point in an absolute minimum.

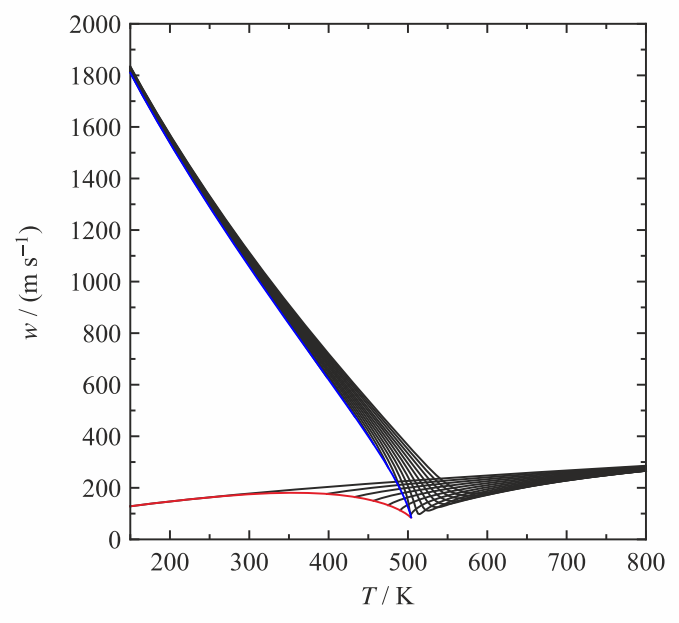

Figure 19. Speed of sound w as a function of temperature along the saturated liquid line (blue), saturated vapor line (red), and isobars (black).

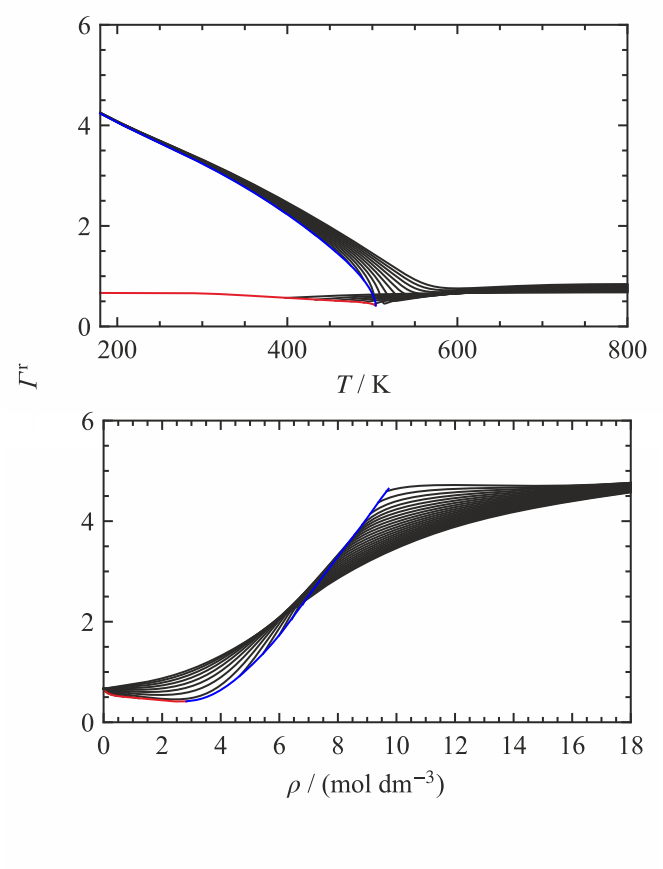

Figure 20. Residual Grüneisen parameter Γ^r as a function of temperature (top) and density (bottom) along the saturated liquid line (blue), saturated vapor line (red), and isobars (top, black), and isotherms (bottom, black).

Another indicator for a reasonable physical behavior is the qualitative form of the residual Grüneisen parameter Γ^r. The Grüneisen parameter [157] was initially introduced for the description of crystalline properties, but later also evaluated for fluids by Arp et al. [158]. Due to its definition as the ratio of the first pressure derivative with respect to temperature at constant density and the isochoric heat capacity, it qualifies for the assessment of the physical behavior of empirical equations of state. In Figure 20, Γ^r is plotted as a function of temperature and density, respectively. Because of the analogous definition to the speed of sound, similar requirements apply for the shape of the saturation lines and isobars, which becomes evident in the plot over temperature. The saturation lines also converge in a distinct minimum at the critical temperature. For high temperatures, the residual Grüneisen parameter exhibits a positive slope and negative curvature. The isotherms in the density dependent plot must show a monotonic course with a positive curvature at low densities and a negative curvature at high densities. The isotherms intersect once above the critical density and run with a positive slope to high densities, without intersecting again. Figure 20 shows the correct behavior of the equation of state.

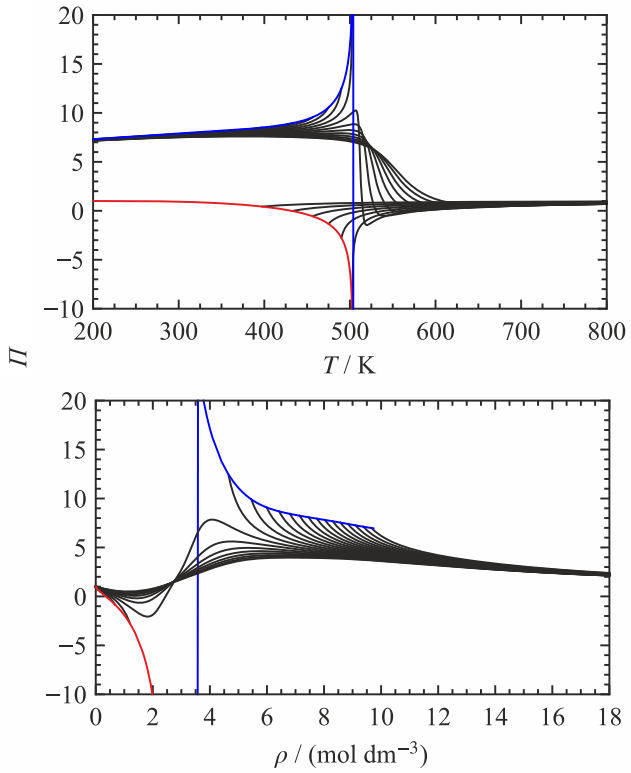

Figure 21. Phase identification parameter [159] Π as a function of temperature (top) and density (bottom) along the saturated liquid line (blue), saturated vapor line (red) and isobars (top, black), and isotherms (bottom, black).

The phase identification parameter Π was introduced by Venkatarathnam and Oellrich [159] as a simple indicator for the aggregation state. Since partial derivatives of pressure, temperature, and density are involved, monitoring this property is a convenient way to identify incorrect behavior Figure 21 shows Π as a function of temperature and density. The course of the saturation lines confirms a correct behavior. Slope and curvature of the saturated liquid line with respect to temperature (cf. Figure 21, top) are positive and negative for the saturated vapor line. In the Π,ρ-diagram, the saturated liquid line exhibits a negative slope, whereas the curvature is positive. Opposing behavior applies for the saturated vapor line. In both diagrams, distinct maxima and minima of the saturated liquid and saturated vapor lines are present. The isobars in the top panel of Figure 21 show almost not curvature at low temperatures. Supercritical isobars intersect in their further course and converge up to high temperatures. Supercritical isotherms in the bottom panel of Figure 21 exhibit a minimum below the critical density and a maximum beyond the critical density. In between, the isotherms should show a single change of curvature.

7. Conclusion

Experimental density and speed of sound data were determined in the liquid phase of 1-hexene. Density measurements were carried out along four isotherms with a vibrating-tube densimeter for temperatures between 300 K and 362 K or pressures of up to 91 MPa. The expanded combined uncertainty is estimated to be 1.0 kg·m^{-3} to 1.1 kg·m^{-3} (k = 2), which corresponds to relative uncertainties of 0.14 % to 0.18 % (k = 2). For speed of sound measurements, two independent apparatuses were utilized, applying the same double-path-length pulse-echo technique. With apparatus 1, the speed of sound was measured along four isotherms in the temperature range from 300 K to 362 K and pressures of up to 91 MPa. The expanded combined uncertainty of apparatus 1 was estimated to be 0.8 m·s^{-1} to 1.2 m·s^{-1} (k = 2), which corresponds to relative uncertainties of 0.08 % to 0.11 % (k = 2). With apparatus 2, the experimentally covered state region for the speed of sound was considerably extended along seven isotherms from temperatures of 215 K to 500 K and pressures of up to 151 MPa. The expanded combined uncertainty for apparatus 2 was estimated to be 0.8 m·s^{-1} to 1.2 m·s^{-1} (k = 2) or 0.07 % to 0.1 % (k = 2), respectively. These data provided an important basis for the development of the fundamental equation of state in terms of the Helmholtz energy for 1-hexene presented in this work.

The equation of state consists of an ideal part, including three Planck-Einstein terms, and a residual part, including five polynomial, five exponential, and five Gaussian bell-shaped terms. It is valid in the fluid region, from the triple point temperature T_{tr} = 133.39 K to T_{max} = 535 K and a maximum pressure of p_{max} = 245 MPa. The uncertainty of different thermodynamic properties calculated with the equation of state was estimated based on the representation of experimental data and their corresponding uncertainties. The uncertainty of homogeneous density data in the liquid phase at atmospheric pressure and temperatures between 270 K and 340 K was estimated to be 0.1 %. For temperatures between 273 K to 333 K at pressures of up to 70 MPa, the uncertainty is 0.1 %. Outside of this range, for temperatures and pressures of up to 360 K and 95 MPa, the uncertainty increases to 0.18 %. No uncertainty estimations for homogeneous vapor, saturated liquid, and saturated vapor densities can be provided due to the lack of reliable experimental data. Vapor pressure data in the temperature range from 273 K to 363 K can be determined with an uncertainty of 0.5 %. The uncertainty with respect to calculated speed of sound data in the homogeneous liquid phase is estimated with 0.15 % in the temperature range from 300 K to 365 K and pressures of up to 90 MPa and 0.2 % for higher pressures of up to 100 MPa and temperatures up to 433 K. Saturation heat capacities in the liquid phase for temperatures between 136 K and 308 K can be calculated with an uncertainty of 0.2 %. No uncertainty estimate for calculated isobaric heat capacities can be provided. The equation of state exhibits reasonable extrapolation and physical behavior in state regions, which are not covered by experimental data.

Table 17: Test values in the homogeneous region, calculated with the present equation of state.

T / K	p / MPa	ρ / (mol·dm^{-3})	c_p / (J·mol^{-1}·K^{-1})	w / (m·s^{-1})	h / (J·mol^{-1})	s / (J·mol^{-1}·K^{-1})	a / (J·mol^{-1})
300	0.002490162	0.001	130.2264437	177.6851621	23687.70871	99.94829959	−8786.943313
300	6.036182516	8	182.8600112	1105.511473	−6538.475027	−22.9515988	−407.518201
450	1.450738906	5.8	257.9030576	403.7924555	25284.94461	63.84057209	−3693.440233
450	0.250858298	0.07	187.3573887	207.5147257	46846.16148	124.0529255	−12561.34495
600	8.033819707	3	304.1341828	197.8662261	66611.43496	140.0031906	−20068.41931

A parameter file for the use in TREND [160] or REFPROP [161] is provided in the supplementary material. In Table 17, test values are given. The number of digits is not related to the uncertainty. Due to the insufficient and qualitatively poor data situation, potential for improvement is seen in the description of the critical region and homogeneous vapor phase for all thermodynamic properties. Furthermore, there is a need for optimization of the description of the isobaric heat capacity at elevated temperatures and pressures. However, this requires new accurate experimental data.

8. References

[1] O. Kunz, W. Wagner, The GERG-2008 Wide-Range Equation of State for Natural Gases and Other Mixtures: An Expansion of GERG-2004, J. Chem. Eng. Data 57 (2012) 3032–3091. https://doi.org/10.1021/je300655b.

[2] AGA Transmission Measurement Committee, Thermodynamic Properties of Natural Gas and Related Gases: GERG-2008 Equation of State, AGA Report No. 8, 3rd ed., Washington, DC, 2017.

[3] T. Neumann, S. Herrig, R. Beckmüller, M. Thol, R. Span, EOS-CG-2021: A Mixture Model for the Calculation of Thermodynamic Properties of CCS Mixtures, unpublished (2022).

[4] M. Thol, M. Richter, E. F. May, E. W. Lemmon, R. Span, EOS-LNG: A Fundamental Equation of State for the Calculation of Thermodynamic Properties of Liquefied Natural Gases, J. Phys. Chem. Ref. Data 48 (2019) 033102. https://doi.org/10.1063/1.5093800.

[5] R. Beckmüller, M. Thol, I. H. Bell, E. W. Lemmon, R. Span, New Equations of State for Binary Hydrogen Mixtures Containing Methane, Nitrogen, Carbon Monoxide, and Carbon Dioxide, J. Phys. Chem. Ref. Data 50 (2021) 013102. https://doi.org/10.1063/5.0040533.

[6] M. T. Gude, A. S. Teja, Measurement Techniques for Critical Properties of Unstable Substances, AIChE Symp.Ser. 90 (1994) 14–22.

[7] J. P. McCullough, H. L. Finke, M. E. Gross, J. F. Messerly, G. Waddington, Low Temperature Calorimetric Studies of Seven 1- Olefins: Effect of Orientation Disorder in the Solid State, J. Phys. Chem. 61 (1957) 289–301. https://doi.org/10.1021/j150549a007.

[8] M. E. Wieser, M. Berglund, Atomic weights of the elements 2007 (IUPAC Technical Report), Pure Appl. Chem. 81 (2009) 2131–2156. https://doi.org/10.1351/PAC-REP-09-08-03.

[9] E. Tiesinga, P. J. Mohr, D. B. Newell, B. N. Taylor, CODATA Recommended Values of the Fundamental Physical Constants: 2018, J. Phys. Chem. Ref. Data 50 (2021) 033105. https://doi.org/10.1063/5.0064853.

[10] Sigma-Aldrich, 1-hexene: MSDS No. 1907/2006 [Online], Taufkirchen, 2021.

[11] A. Behr, D. W. Agar, J. Jörissen, Einführung in die Technische Chemie, 2nd ed., Spektrum Akademischer Verlag, Heidelberg, 2009. 9783827421951. https://doi.org/10.1007/978-3-662-52856-3.

[12] National Center for Biotechnology Information, PubChem Compound Summary for CID 11597, 1-Hexene, 2022, https://pubchem.ncbi.nlm.nih.gov/compound/1-Hexene, accessed 2 February 2022.

[13] Chevron Phillips Chemical Company LP, Safe Handling & Storage of AlphaPlus® 1-Hexene and AlphaPlus® 1-Octene, 2013.

[14] M. A. Javed, M. Rüther, E. Baumhögger, J. Vrabec, Density and Thermodynamic Speed of Sound of Liquid Vinyl Chloride, J. Chem. Eng. Data 65 (2020) 2495–2504. https://doi.org/10.1021/acs.jced.9b01133.

[15] Anton Paar GmbH, Instruction Manual DMA HPM: Density Measuring Cell for High Pressures and High Temperatures, Graz, Austria, 2012.

[16] E. W. Lemmon, M. O. McLinden, W. Wagner, Thermodynamic Properties of Propane. III. A Reference Equation of State for Temperatures from the Melting Line to 650 K and Pressures up to 1000 MPa, J. Chem. Eng. Data 54 (2009) 3141–3180. https://doi.org/10.1021/je900217v.

[17] W. Wagner, A. Pruß, The IAPWS Formulation 1995 for the Thermodynamic Properties of Ordinary Water Substance for General and Scientific Use, J. Phys. Chem. Ref. Data 31 (2002) 387–535. https://doi.org/10.1063/1.1461829.

[18] M. A. Javed, E. Baumhögger, J. Vrabec, Thermodynamic Speed of Sound Data for Liquid and Supercritical Alcohols, J. Chem. Eng. Data 64 (2019) 1035–1044. https://doi.org/10.1021/acs.jced.8b00938.

[19] M. A. Javed, E. Baumhögger, J. Vrabec, Thermodynamic speed of sound of xenon, J. Chem. Thermodyn. 141 (2020) 105933. https://doi.org/10.1016/j.jct.2019.105933.

[20] M. Altschul, Über die kritischen Grössen einiger organischen Verbindungen, Z. Phys. Chem. 11U (1893) 577–597. https://doi.org/10.1515/zpch-1893-1143.

[21] W. Herz, Über die Regeln von Guldberg und Trouton-Nernst in homologen Reihen von Verbindungen, Z. Anorg. Allg. Chem. 95 (1916) 253–256. https://doi.org/10.1002/zaac.19160950117.

[22] D. Ambrose, J. D. Cox, R. Townsend, The critical temperatures of forty organic compounds, Trans. Faraday Soc. 56 (1960) 1452–1459. https://doi.org/10.1039/tf9605601452.

[23] R. R. Dreisbach, Physical Properties of Chemical Compounds, American Chemical Society, Washington, District of Columbia, 1961. 0841224498. https://doi.org/10.1021/ba-1959-0022.ch001.

[24] W. B. Kay, C. L. Young, Selected Data on Mixtures, Int. Data Series Sel. Data Mixtures Ser. A 3 (1974) 192–201.

[25] R. C. Reid, J. M. Prausnitz, B. E. Poling, The Properties of Gases and Liquids, 5th ed., McGraw-Hill, New York, 1987. https://doi.org/10.1036/0070116822.

[26] M. T. Gude, D. J. Rosenthal, A. S. Teja, The critical properties of 1-alkenes from 1-pentene to 1-dodecene, Fluid Phase Equilib. 70 (1991) 55–64. https://doi.org/10.1016/0378-3812(91)85004-E.

[27] P. Ma, Z. Fang, J. Zhang, Y. Ruan, Determination of Critical Constants, Saturated Vapor or Liquid Densities and Vapor Pressures of Six Organic Compounds, Chin. J. Chem. Eng. 6 (1992) 112–117.

[28] Y. Li, P. Ma, Measurement of the Critical Constants of 1-Hexene and 1-Bromopropane., Shiyou-huagong 22 (1993) 322–327.

[29] D. R. Lide, H. V. Kehiaian, CRC handbook of thermophysical and thermochemical data, 1st ed., CRC Press, Boca Raton, 1994. 0849301971. https://doi.org/10.1201/9781003067719.

[30] V. V. Zotov, Yu. F. Melikhov, G. A. Mel'nikov, Yu. A. Neruchev, Skorost' zvuka v zhidkikh uglevodorodakh: (The Sound Velocity in Liquid Hydrocarbons), Kursk, 1995. 9785883130747.

[31] C. Tsonopoulos, D. Ambrose, Vapor−Liquid Critical Properties of Elements and Compounds. 6. Unsaturated Aliphatic Hydrocarbons, J. Chem. Eng. Data 41 (1996) 645–656. https://doi.org/10.1021/je9501999.

[32] J. E. Kilpatrick, E. J. Prosen, K. S. Pitzer, F. D. Rossini, Heats, equilibrium constants, and free energies of formation of the monoolefin hydrocarbons, J. Res. Natl. Bur. Stand. (U. S.) 36 (1946) 559–612. https://doi.org/10.6028/jres.036.034.

[33] E. W. Lemmon, R. T. Jacobsen, A New Functional Form and New Fitting Techniques for Equations of State with Application to Pentafluoroethane (HFC-125), J. Phys. Chem. Ref. Data 34 (2005) 69–108. https://doi.org/10.1063/1.1797813.

[34] D. Vega-Maza, M. C. Martín, J. P. M. Trusler, J. J. Segovia, Heat capacities and densities of the binary mixtures containing ethanol, cyclohexane or 1-hexene at high pressures, J. Chem. Thermodyn. 57 (2013) 550–557. https://doi.org/10.1016/j.jct.2012.07.018.

[35] G. A. Torín-Ollarves, J. J. Segovia, M. C. Martín, M. A. Villamañán, Density, Viscosity, and Isobaric Heat Capacity of the Mixture (1-Butanol + 1-Hexene), J. Chem. Eng. Data 58 (2013) 2717–2723. https://doi.org/10.1021/je301301j.

[36] B. Lagourette, C. Boned, H. Saint-Guirons, P. Xans, H. Zhou, Densimeter calibration method versus temperature and pressure, Meas. Sci. Technol. 3 (1992) 699–703. https://doi.org/10.1088/0957-0233/3/8/002.

[37] A. K. Abas-Zade, A. M. Kerimov, N. A. Agaev, T. A. Apaev, Experimental Determination of Density of Hydrocarbons, Teplofiz. Svoistva Zhidk. (1970) 34–38.

[38] I. Abala, M. Lifi, F. E. M'hamdi Alaoui, N. Munoz-Rujas, F. Aguilar, E. A. Montero, Thermophysical Property Measurements and Modeling of (Ether + Alkanol + Hydrocarbon) Mixtures: Binary and Ternary Mixtures (Dibutyl Ether + 1-Butanol + 1-Hexene or + Iso-octane) at 298.15 K, J. Chem. Eng. Data 66 (2021) 3417–3431. https://doi.org/10.1021/acs.jced.1c00157.

[39] E. Aicart, E. Junquera, T. M. Letcher, Isobaric thermal expansivity and isothermal compressibility of several nonsaturated hydrocarbons at 298.15 K, J. Chem. Eng. Data 40 (1995) 1225–1227. https://doi.org/10.1021/je00022a017.

[40] D. Belhadj, A. Negadi, A. Hernández, I. Mokbel, I. Bahadur, L. Negadi, A study on mixing properties of binary mixtures of 1-hexene with alkoxyethanols at different temperatures, J. Chem. Thermodyn. 172 (2022) 106820. https://doi.org/10.1016/j.jct.2022.106820.

[41] M. M. Bourguel, Sur quelques carbures éthyléniques obtenus par semi-réduction des acétylèniques, Bull. Soc. Chim. Fr. 41 (1927) 1475–1479.

[42] R. Bravo, M. Pintos, A. Amigo, Excess molar volumes of (o-xylene + n-heptane + toluene or n-hex-1-ene) at the temperature 298.15 K, J. Chem. Thermodyn. 23 (1991) 905–910. https://doi.org/10.1016/S0021-9614(05)80171-5.

[43] R. Bravo, M. Pintos, A. Amigo, Excess Molar Volumes at the Temperature 308.15 K of the Ternary Mixtures (o -Xylene + n -Heptane + Toluene Or n -Hex-1-Ene), Phys. Chem. Liq. 24 (1992) 239–248. https://doi.org/10.1080/00319109208027275.

[44] K. N. Campbell, L. T. Eby, The Reduction of Multiple Carbon—Carbon Bonds. III. Further Studies on the Preparation of Olefins from Acetylenes, J. Am. Chem. Soc. 63 (1941) 2683–2685. https://doi.org/10.1021/ja01855a050.

[45] K. N. Campbell, M. J. O'Connor, The Hydrogenation of Substituted Acetylenes with Raney Nickel, J. Am. Chem. Soc. 61 (1939) 2897–2900. https://doi.org/10.1021/ja01265a090.

[46] Y. Chen, C. Liu, Determination and correlation of liquid- liquid equilibrium data for toluene -n- hexene -dimethyl sulfoxide system, Huagong Xuebao/CIESC J. 64 (2013) 814–819.

[47] R. M. de Fré, L. A. Verhoeye, Phase equilibria in systems composed of an aliphatic and an aromatic hydrocarbon and sulpholane, J. Appl. Chem. 26 (1976) 469–487. https://doi.org/10.1002/jctb.5020260168.

[48] D. H. Desty, F. A. Fidler, Azeotrope Formation between Sulfur Compounds and Hydrocarbons, Ind. Eng. Chem. 43 (1951) 905–910. https://doi.org/10.1021/ie50496a037.

[49] J. Dojčanský, J. Heinrich, J. Surový, Izotermická rovnováha kvapalina - para v sústave 1-hexén - benzén pri teplote 25 °C, Chem. Zvesti 21 (1967) 713–717.

[50] M. G. Fomina, Viscosity and density of ethylene hydrocarbons, their binary and multicomponent mixtures at pressures up to 245 MPa and temperatures up to 473 K. Ph.D. Thesis, Kazan, 1986.

[51] A. F. Forziati, D. L. Camin, F. D. Rossini, Density, refractive index, boiling point, and vapor pressure of eight monoolefin (1-alkene), six pentadiene, and two cyclomonoolefin hydrocarbons, J. Res. Natl. Bur. Stand. (U. S.) 45 (1950) 406–410. https://doi.org/10.6028/jres.045.044.

[52] F. H. Garner, R. Wilkinson, A. W. Nash, The Knock Rating of Δα-Olefines. A Contribution to the study of the Significance of Olefines in Cracked Petrol, J. Soc. Chem. Ind. Trans. Comm. 15 (1932) 265–271. https://doi.org/10.1002/jctb.5000513307.

[53] N. Gee, K. Shinsaka, J.-P. Dodelet, G. R. Freeman, Dielectric constant against temperature for 43 liquids, J. Chem. Thermodyn. 18 (1986) 221–234. https://doi.org/10.1016/0021-9614(86)90050-9.

[54] G. Geiseler, E. Pilz, Zur Kenntnis der Dipolmomente homologer α-Olefine, Chem. Ber. 95 (1962) 96–101. https://doi.org/10.1002/cber.19620950118.

[55] S. O. Guseinov, Z. S. Galandarov, Investigation of the Density of 1-hexene at low Temperatures and Pressures, Izv. Vyssh. Uchebn. Zaved. Neft Gaz 25 (1982) 66–68.

[56] R. N. Hollenshead, M. van Winkle, Relative Volatility of the Hexane-C 6 Olefin Systems in N,N-Dimethylformamide, J. Chem. Eng. Data 11 (1966) 420–423. https://doi.org/10.1021/je60030a041.

[57] G. H. Jeffery, A. I. Vogel, 133. Physical properties and chemical constitution. Part XVI. Ethylenic compounds, J. Chem. Soc. 2 (1948) 658–673. https://doi.org/10.1039/jr9480000658.

[58] A. M. Kerimov, T. A. Apaev, Experimental values of density for hexene-1, octene-1, cyclohexane, and methylcyclohexane in varying temperatures and pressures., Teplofiz. Svoistva Vesh. Mater. 5 (1972) 26–46.

[59] F. Krollpfeiffer, H. Seebaum, Über die Gasbenzine der Schwelanlage der Gelsenkirchener Bergwerks-A.G, J.

Prakt. Chem. 119 (1928) 131–156. https://doi.org/10.1002/prac.19281190111.

[60] L. S. Kudryavtseva, K. Viit, O. G. Eizen, Liquid-Vapor Equilibrium in Binary Systems, forming during the Synthesis of α-Alkenes, Eesti NSV Tead. Akad. Toim. Keem. Geol. 17 (1968) 242–250.

[61] L. S. Kudryavtseva, H. Viit, O. G. Eizen, Liquid-Vapor Equilibrium in Binary Systems containing Olefins, Eesti NSV Tead. Akad. Toim. Keem. Geol. 18 (1969) 346–352.

[62] L. S. Kudryavtseva, H. H. Kirss, O. G. Eisen, Ein Verfahren zur Berechnung der Dampfzusammensetzung von ternären flüssigen Systemen, Monatsh. Chem. 105 (1974) 19–29. https://doi.org/10.1007/BF00911283.

[63] T. M. Lesteva, G. I. Logunova, V. I. Chernaya, Certain Physicochemical Properties of Hex-1-ene-Solvent Systems, Zh. Fiz. Khim. 53 (1979) 1180–1183.

[64] T. M. Letcher, The excess volumes of some mixtures of saturated and unsaturated C6 hydrocarbons, J. Chem. Thermodyn. 7 (1975) 205–209. https://doi.org/10.1016/0021-9614(75)90057-9.

[65] T. M. Letcher, The excess volumes of some mixtures of saturated and unsaturated C6 hydrocarbons. Part II, J. Chem. Thermodyn. 9 (1977) 661–664. https://doi.org/10.1016/0021-9614(77)90091-X.

[66] T. M. Letcher, F. Marsicano, Thermodynamics of hydrocarbon mixtures using gas-liquid chromatography The determination of activity coefficients of some unsaturated C5 and C6 unbranched hydrocarbons in n-octadecane, n-octadec-1-ene, n-hexadecane, and n-hexadec-1-ene, J. Chem. Thermodyn. 6 (1974) 501–507. https://doi.org/10.1016/0021-9614(74)90012-3.

[67] T. M. Letcher, P. Reddy, Ternary liquid–liquid equilibria for mixtures of 1-hexyl-3-methylimidozolium (tetrafluoroborate or hexafluorophosphate) + ethanol + an alkene at T=298.2K, Fluid Phase Equilib. 219 (2004) 107–112. https://doi.org/10.1016/j.fluid.2003.10.012.

[68] M. Lifi, J. Lorenzo, F. Aguilar, N. Muñoz-Rujas, E. A. Montero, Y. Chhiti, F. E. M. Alaoui, Excess enthalpy, density, speed of sound and refractive index of binary mixtures {2-(2-ethoxyethoxy)ethanol + 1-hexene, or cyclohexane, or methylcyclohexane at (298.15 and 313.15) K: Application of the PPR-78 cubic equation of state, NRTL and UNIQUAC models, The Journal of Chemical Thermodynamics 153 (2021) 106306. https://doi.org/10.1016/j.jct.2020.106306.

[69] B. Marrufo, A. Aucejo, M. Sanchotello, S. Loras, Isobaric vapor–liquid equilibrium for binary mixtures of 1-hexene + n-hexane and cyclohexane + cyclohexene at 30, 60 and 101.3 kPa, Fluid Phase Equilib. 279 (2009) 11–16. https://doi.org/10.1016/j.fluid.2008.12.007.

[70] J. C. McCoubrey, J. N. McCrea, A. R. Ubbelohde, The configuration of flexible polymethylene molecules in the gas phase, J. Chem. Soc. 439 (1951) 1961–1971. https://doi.org/10.1039/jr9510001961.

[71] T. W. Mears, A. Fookson, P. Pomerantz, E. H. Rich, C. S. Dussinger, F. L. Howard, Syntheses and properties of two olefins, six paraffins, and their intermediates, J. Res. Natl. Bur. Stand. (U. S.) 44 (1950) 299–311. https://doi.org/10.6028/jres.044.027.

[72] Yu. F. Melikhov, G. A. Mel'nikov, V. M. Tutov, V. N. Verveiko, Accoustic and thermal properties of some hexane derivatives at high state parameters., Izv. Vyssh. Uchebn. Zaved. Energ. 34 (1991) 73–78.

[73] S. M. Nazmul Hasan, Excess Molar Enthalpies of Binary and Ternary Systems Involving Hydrocarbons and Ethers. Master Thesis, Saskatoon, 2010.

[74] S. K. Ogorodnikov, V. B. Kogan, M. S. Nemtsov, Liquid - Vapor Equilibrium in Binary Systems of Hydrocarbons with Acetone, Russ. J. Appl. Chem. 34 (1961) 323–331.

[75] C. A. Ohlin, P. J. Dyson, G. Laurenczy, Carbon monoxide solubility in ionic liquids, Chem. Comm. (2004) 1070–1071. https://doi.org/10.1039/b401537a.

[76] I. B. Pukinskii, G. G. Chernik, G. O. Chistyakova, N. A. Smirnova, Investigation and calculation of the phase equilibrium in the systems hexene-propanol-water and heptene-propanol-water., Khim. Termodin. Rastvorov Leningrad (1982) 157–178.

[77] H. Renon, J. M. Prausnitz, Liquid-Liquid and Vapor-Liquid Equilibria for Binary and Ternary Systems with Dibutyl Ketone, Dimethyl Sulfoxide, n -Hexane, and 1-Hexene, Ind. Eng. Chem. Proc. Des. Dev. 7 (1968) 220–225. https://doi.org/10.1021/i260026a011.

[78] D. I. Sagdeev, M. G. Fomina, G. K. Mukhamedzyanov, I. M. Abdulagatov, Experimental Study and Correlation Models of the Density and Viscosity of 1-Hexene and 1-Heptene at Temperatures from (298 to 473) K and Pressures up to 245 MPa, J. Chem. Eng. Data 59 (2014) 1105–1119. https://doi.org/10.1021/je401015e.

[79] Y. S. Suryanarayana, M. van Winkle, Solvent Effect on Relative Volatility. n-Hexane-Hexene-1 System., J. Chem. Eng. Data 11 (1966) 7–12. https://doi.org/10.1021/je60028a002.

[80] G. Tardajos, M. Diaz Pena, A. Lainez, E. Aicart, Speed of sound in and isothermal compressibility and isobaric expansivity of pure liquids at 298.15 K, J. Chem. Eng. Data 31 (1986) 492–493. https://doi.org/10.1021/je00046a031.

[81] J. Tojo, C. Diaz, Densities and Refractive Indices for 1-Hexene + o-Xylene, + m-Xylene, + p-Xylene, and + Ethylbenzene, J. Chem. Eng. Data 40 (1995) 96–98. https://doi.org/10.1021/je00017a021.

[82] A. J. Treszczanowicz, T. S. Pawłowski, T. Treszczanowicz, Temperature dependence of the excess molar volume of 1-hexanol+1-alkene systems in terms of an association and equation of state model, Fluid Phase Equilib. 295 (2010) 155–162. https://doi.org/10.1016/j.fluid.2010.04.011.

[83] A. J. Treszczanowicz, T. S. Pawłowski, T. Treszczanowicz, A. M. Szafrański, Excess Volume of the 1-Propanol + 1-Alkene Systems in Terms of an Equation of State with Association, J. Chem. Eng. Data 55 (2010) 5478–5482. https://doi.org/10.1021/je100595s.

[84] J. von Braun, Über den Zerfall quartärer Ammoniumhydroxyde, Justus Liebigs Ann. Chem. 382 (1911) 1–49. https://doi.org/10.1002/jlac.19113820102.

[85] Z. Wang, G. C. Benson, B. C.-Y. Lu, Excess enthalpies of binary mixtures of 1-hexene with some branched alkanes at the temperature 298.15 K, J. Chem. Thermodyn. 36 (2004) 45–47. https://doi.org/10.1016/j.jct.2003.09.004.

[86] A. Weissler, V. A. Del Grosso, Ultrasonic Investigation of Liquids. VI. Acetylene Derivatives, J. Am. Chem. Soc. 72 (1950) 4209–4210. https://doi.org/10.1021/ja01165a107.

[87] J. P. Wibaut, H. Geldof, Accurate values of the specific gravities and the refractive indices of a series of alkenes with terminal double bond, Recl. Trav. Chim. Pays-Bas 65 (1946) 125–126. https://doi.org/10.1002/recl.19460650211.

[88] R. Wilkinson, CCCCXXII.—Studies in the olefin series. Part I. The synthesis of Δ 1 -olefins, J. Chem. Soc. (1931) 3057–3062. https://doi.org/10.1039/JR9310003057.

[89] F. J. Wright, Latent Heat of Vaporisation and Composition, Recl. Trav. Chim. Pays-Bas 79 (1960) 784–789. https://doi.org/10.1002/recl.19600790803.

[90] J. Yang, X. Meng, J. Wu, Liquid Density of n -Pentene, n -Hexene, and n -Heptene at Temperatures from 283.15 to 363.15 K and Pressures up to 100 MPa, J. Chem. Eng. Data 63 (2018) 2280–2289. https://doi.org/10.1021/acs.jced.8b00229.

[91] Z. I. Zaripov, G. K. Mukhamedzyanov, S. A. Bulaev, Thermal conductivity, thermal diffusivity, and heat capacity of unsaturated hydrocarbons at pressures up to 200 MPa, High Temp. 48 (2010) 132–135. https://doi.org/10.1134/S0018151X10010177.

[92] V. V. Zotov, B. N. Kireev, Yu. A. Neruchev, Study of the Equilibria Properties of Hydrocarbons on the Coexistence Curve Using Acoustic Method., Prikl. Mekh. Tekh. Fiz. 2 (1975) 162–164.

[93] Dortmund Data Bank, 2021, www.ddbst.com, accessed 22 September 2021.

[94] D. I. Sagdeev, M. G. Fomina, G. Mukhamedzyanov, I. M. Abdulagatov, Experimental study of the density and viscosity of polyethylene glycols and their mixtures at temperatures from 293K to 473K and at atmospheric pressure, J. Chem. Thermodyn. 43 (2011) 1824–1843. https://doi.org/10.1016/j.jct.2011.06.013.

[95] B. N. Kireev, Determination of the density of olefins along the saturation line, Nauchn. Tr. Kursk. Gos. Pedagog. Inst 23 (1974) 40–45.

[96] M. Frenkel, R. D. Chirico, V. Diky, K. Kroenlein, C. D. Muzny, A. F. Kazakov, J. W. Magee, I. M. Abdulagatov, E. W. Lemmon, ThermoData Engine, NIST Standard Reference Database 103b, version 10.4.2, National Institute of Standards and Technology, Gaithersburg, 2021.

[97] N. S. Osborne, C. H. Meyers, A formula and tables for the pressure of saturated water vapor in the range 0 to 374 C, J. Res. Natl. Bur. Stand. (U. S.) 13 (1934) 1. https://doi.org/10.6028/jres.013.003.

[98] L. Negadi, A. Blondel, I. Mokbel, A. Ait-Kaci, J. Jose, Liquid-vapor equilibria, excess Gibbs energies, and excess volumes of dimethyl carbonate + heptane, + 1-hexene, + cyclohexane, or + benzene, Int. Data Series Sel. Data Mixtures Ser. A 21 (1993) 169–194.

[99] L. Negadi, H. Delepine, A. Ait-Kaci, J. Jose, Static Measurements of the Total Vapor Pressure of Binary Mixtures of Dimethyl Carbonate+ Hex-1-yne, Hex-2-yne, Hex-3-yne, Cyclohexane, Hex-1-ene, or Heptane at Temperatures Between 263 and 373 K, Eldata Int. Electron. J. Phys. - Chem. Data 5 (1999) 197–210.

[100] L. Negadi, A. Belabbaci, A. Ait Kaci, J. Jose, Isothermal Vapor−Liquid Equilibria and Excess Enthalpies of (Propyl Ethanoate + Heptane), (Propyl Ethanoate + Cyclohexane), and (Propyl Ethanoate + 1-Hexene), J. Chem. Eng. Data 52 (2007) 47–55. https://doi.org/10.1021/je060184i.

[101] E. Sapei, A. Zaytseva, P. Uusi-Kyyny, K. I. Keskinen, J. Aittamaa, Vapor−Liquid Equilibrium for Binary

System of Thiophene + n -Hexane at (338.15 and 323.15) K and Thiophene + 1-Hexene at (333.15 and 323.15) K, J. Chem. Eng. Data 51 (2006) 2203–2208. https://doi.org/10.1021/je0603022.

[102] H. Segura, E. Lam, R. Reich, J. Wisniak, Isobaric Phase Equilibria in the Binary Systems Ethyl 1,1-Dimethylethyl Ether + 1-hexene and + Cyclohexene at 94.00 kPa, Chem. Phys. 39 (2001) 43–54. https://doi.org/10.1080/00319100108030325.

[103] D. L. Camin, F. D. Rossini, Physical Properties of the 17 Isomeric Hexenes of the API Research Series, J. Phys. Chem. 60 (1956) 1446–1451. https://doi.org/10.1021/j150544a029.

[104] C. Alonso-Tristán, M. A. Villamañán, C. R. Chamorro, J. J. Segovia, Phase Equilibrium Properties of Binary and Ternary Mixtures Containing Dibutyl Ether, Cyclohexane, and Heptane or 1-Hexene at T = 313.15 K, J. Chem. Eng. Data 53 (2008) 1486–1491. https://doi.org/10.1021/je7007523.

[105] D. Ambrose, B. E. Broderick, R. Townsend, The critical temperatures and pressures of thirty organic compounds, J. Appl. Chem. 24 (1974) 359–372. https://doi.org/10.1002/jctb.5020240607.

[106] A. Belabbaci, S. Ghellai, R. M. Villamañán, M. C. Martín, L. Negadi, M. A. Villamañán, Phase equilibrium properties of binary and ternary mixtures containing 2-butanol, 2,2,4-trimethylpentane and 1-hexene at 313.15K, Fluid Phase Equilib. 369 (2014) 33–38. https://doi.org/10.1016/j.fluid.2014.02.018.

[107] A. Belabbaci, C. Ghezouali, R. M. Villamañán, J. J. Segovia, M. A. Villamañán, L. Negadi, Isothermal vapor–liquid equilibrium and molar excess Gibbs energies of two ternary systems containing either 1-butanol or 2-butanol+1-hexene+methylbenzene at 313.15K, Fluid Phase Equilib. 386 (2015) 1–6. https://doi.org/10.1016/j.fluid.2014.11.010.

[108] L. S. Budantseva, T. M. Lesteva, M. S. Nemtsov, Azeotrope Formation in Methanol-Water-Hydrocarbon Systems, Viniti (1973) 1–8.

[109] C. R. Chamorro, J. J. Segovia, M. C. Martín, E. A. Montero, M. A. Villamañán, Phase equilibrium properties of binary and ternary systems containing tert-amylmethyl ether (TAME) as oxygenate additive and gasoline substitution hydrocarbons at 313.15 K, Fluid Phase Equilib. 156 (1999) 73–87. https://doi.org/10.1016/S0378-3812(99)00033-3.

[110] C. R. Chamorro, J. J. Segovia, M. C. Martín, M. A. Villamañán, Vapor–liquid equilibrium of octane-enhancing additives in gasolines, Fluid Phase Equilib. 193 (2002) 289–301. https://doi.org/10.1016/S0378-3812(01)00751-8.

[111] C. R. Chamorro, M. C. Martín, M. A. Villamañán, J. J. Segovia, Characterization and modelling of a gasoline containing 1,1-dimethylethyl methyl ether (MTBE), diisopropyl ether (DIPE) or 1,1-dimethylpropyl methyl ether (TAME) as fuel oxygenate based on new isothermal binary vapour–liquid data, Fluid Phase Equilib. 220 (2004) 105–112. https://doi.org/10.1016/j.fluid.2004.02.013.

[112] K. Fischer, J. Gmehling, Vapor-liquid equilibria, activity coefficients at infinite dilution and heats of mixing for mixtures of N-methyl pyrrolidone-2 with C5 or C6 hydrocarbons and for hydrocarbon mixtures, Fluid Phase Equilib. 119 (1996) 113–130. https://doi.org/10.1016/0378-3812(95)02983-4.

[113] S. Ghellai, A. Belabbaci, R. M. Villamañán, M. C. Martín, M. A. Villamañán, L. Negadi, Vapour–liquid

equilibria of binary and ternary mixtures containing 1-butanol, 2,2,4-trimethylpentane and 1-hexene at T=313.15K, J. Chem. Thermodyn. 63 (2013) 164–168. https://doi.org/10.1016/j.jct.2013.04.003.

[114] J. Gmehling, Isothermal vapor-liquid equilibriums in binary systems formed by esters with alkenes, J. Chem. Eng. Data 28 (1983) 27–30. https://doi.org/10.1021/je00031a008.

[115] R. Hani, R. Solimando, L. Negadi, J. Jose, A. Ait Kaci, Isothermal (vapor+liquid) equilibria and excess enthalpy data of {1-hexene+methyl butyl ether (MBE)} and {1-hexene+methyl tert-butyl ether (MTBE)} binary systems at several temperatures, J. Chem. Thermodyn. 54 (2012) 83–89. https://doi.org/10.1016/j.jct.2012.03.016.

[116] D. O. Hanson, M. van Winkle, Alteration of the relative volatility of hexane-1-hexene by oxygenated and chlorinated solvents, J. Chem. Eng. Data 12 (1967) 319–325. https://doi.org/10.1021/je60034a009.

[117] R. Hirawan, S. Sinha, S. A. Iwarere, J. D. Raal, P. Naidoo, D. Ramjugernath, Vapor–Liquid Equilibrium Data for 1-Methyl-2-Pyrrolidone + (1-Butanol or 1-Hexene or Water) Binary Mixtures, J. Chem. Eng. Data 59 (2014) 1643–1650. https://doi.org/10.1021/je500092v.

[118] J. L. Humphrey, M. van Winkle, Vapor-liquid equilibrium at 60.degree. for n-hexane-alkyl amines and 1-hexene-alkyl amines, J. Chem. Eng. Data 12 (1967) 526–531. https://doi.org/10.1021/je60035a018.

[119] A. Jabłoniec, S. Horstmann, J. Gmehling, Experimental Determination and Calculation of Gas Solubility Data for Nitrogen in Different Solvents, Ind. Eng. Chem. Res. 46 (2007) 4654–4659. https://doi.org/10.1021/ie061258m.

[120] A. W. Jackowski, Liquid-vapour equilibria in {xCH2Cl2 + (1 − x)C4H9CHCH2} at 298.17 K, J. Chem. Thermodyn. 17 (1985) 765–768. https://doi.org/10.1016/0021-9614(85)90107-7.

[121] A. Jonasson, M. Savoia, O. Persson, A. Fredenslund, Isothermal vapor-liquid equilibrium data for ether + glycol, chloroalkene + glycol, epoxy ether + alkane, epoxy ether + alkene, and epoxy ether + chloroalkane systems, J. Chem. Eng. Data 39 (1994) 134–139. https://doi.org/10.1021/je00013a038.

[122] H. Kirss, L. S. Kudryavtseva, O. G. Eizen, Vapor-liquid equilibrium in ternary systems hexene-1-hexane-octane, benzene-heptene-1-heptane, heptene-1-heptane-toluene and in the corresponding binary systems at a temperature of 55°C, Eesti NSV Tead. Akad. Toim. Keem. Geol. 24 (1975) 15–23.

[123] H. Koch, H. G. van Raay, Binäre azeotrope Mischungen von Methylacetat mit 28 Kohlenwasserstoffen des C5-, C6 - und C7-Bereichs*), Brennst.-Chem. 35 (1954) 105–112.

[124] T. M. Lesteva, V. I. Chernaya, L. A. Rogozilnikova, A. Yu. Evstigneev, Liquid-vapor equilibrium in the system the component 4,4-dimethyldioxane-1,3, Prom. Sint. Kauch. Rezin. Tekh. Izdel. 4 (1985) 6–7.

[125] T. M. Letcher, M. K. Kozłowska, U. Domańska-Żelazna, The determination of activity coefficients at infinite dilution using g.l.c. for hydrocarbons in furfural at T=278.15 K and T=298.15 K, J. Chem. Thermodyn. 36 (2004) 37–40. https://doi.org/10.1016/j.jct.2003.09.011.

[126] L. M. Lozano, E. A. Montero, M. C. Martín, M. A. Villamañán, Isothermal vapor-liquid equilibria of

binary mixtures containing methyl tert-butyl ether (MTBE) and / or substitution hydrocarbons, Fluid Phase Equilib. 133 (1997) 155–162. https://doi.org/10.1016/S0378-3812(97)00010-1.

[127] P. Moodley, Vapour-Liquid Equilibria Studies for Binary Systems containing 1-Hexene and n-Hexane. Master Thesis, KwaZulu-Natal, 2009.

[128] E. Sapei, A. Zaytseva, P. Uusi-Kyyny, K. I. Keskinen, J. Aittamaa, Vapor−Liquid Equilibrium for Binary System of Diethyl Sulfide + n -Hexane at (338.15 and 323.15) K and Diethyl Sulfide + 1-Hexene at (333.15 and 323.15) K, J. Chem. Eng. Data 52 (2007) 571–576. https://doi.org/10.1021/je060460t.

[129] J. J. Segovia, Investigación Termodinámica Del Equilibrio De Fases Fluidas De Mezclas Ternarias Constituidas Por Los Aditivos Oxigenados Mtbe Y Me-tanol Con Hidrocarburos De Sustitución Para El Desarrollo De Nuevas Gasolinas Sin Plomo. Ph. D. Thesis, Spain, 1997.

[130] J. J. Segovia, M. C. Martín, C. R. Chamorro, M. A. Villamañán, Vapor−Liquid Equilibrium of Ternary Mixtures Containing Methyl tert -Butyl Ether and/or Substitution Hydrocarbons. Methyl tert -Butyl Ether + Heptane + Cyclohexane and Methyl tert -Butyl Ether + Cyclohexane + 1-Hexene at 313.15 K, J. Chem. Eng. Data 43 (1998) 1021–1026. https://doi.org/10.1021/je980108i.

[131] D. Tassios, M. van Winkle, Prediction of binary vapor-liquid equilibria. Members of homologous series and a common solvent, J. Chem. Eng. Data 12 (1967) 555–561. https://doi.org/10.1021/je60035a023.

[132] J. Timmermans, La température de fusion des corps organiques., Bull. Soc. Chim. Belg. 36 (1927) 502–508.

[133] J. H. Vera, J. M. Prausnitz, Vapor-Liquid Equilibria in Binary Aromatic-Olefin Systems, J. Chem. Eng. Data 16 (1971) 149–154. https://doi.org/10.1021/je60049a012.

[134] R. M. Villamañán, D. Vega-Maza, C. R. Chamorro, M. A. Villamañán, J. J. Segovia, Thermodynamics of Fuels with a Biosynthetic Component. II. Vapor–Liquid Equilibrium Data for Binary and Ternary Mixtures Containing Ethyl 1,1-Dimethylethyl Ether, 1-Hexene, and Cyclohexane at T = 313.15 K, J. Chem. Eng. Data 53 (2008) 247–251. https://doi.org/10.1021/je7005488.

[135] R. M. Villamañán, J. J. Segovia, M. Carmen Martín, D. Vega-Maza, C. R. Chamorro, M. A. Villamañán, Thermodynamics of fuels with a bio-synthetic component (IV), J. Chem. Thermodyn. 41 (2009) 189–192. https://doi.org/10.1016/j.jct.2008.09.020.

[136] J. von Braun, W. Teuffert, K. Weißbach, Über den Zerfall quartärer Ammonium- und Sulfoniumhydroxyde. IV, Justus Liebigs Ann. Chem. 472 (1929) 121–142. https://doi.org/10.1002/jlac.19294720104.

[137] A. E. Wentink, N. J. M. Kuipers, A. B. de Haan, J. Scholtz, H. Mulder, Effects of Ligand Structure on Reactive Vapor−Liquid Distribution Ratio and Selectivity for C6-Olefin Isomers, Ind. Eng. Chem. Res. 44 (2005) 9221–9229. https://doi.org/10.1021/ie050236h.

[138] J. Wisniak, E. Gabai, Isobaric Vapor−Liquid Equilibria in the Systems Methyl Acetate + 1-Hexene and 1-

Hexene + 2-Propanol, J. Chem. Eng. Data 41 (1996) 143–146. https://doi.org/10.1021/je950211x.

[139] M. A. Y. Torres, S. B. Bottini, E. A. Brignole, V. Sanhueza, R. Reich, Vapor-liquid equilibria for binary mixtures with anisole, Fluid Phase Equilib. 71 (1992) 85–98. https://doi.org/10.1016/0378-3812(92)85006-T.

[140] T. S. Khasanshin, O. G. Poddubskii, A. P. Shchemelev, Sound Velocity in Liquid 1-Alkenes, High Temp. 43 (2005) 530–537. https://doi.org/10.1007/s10740-005-0094-4.

[141] A. L. Badalyan, N. F. Otpushchennikov, Some thermodynamic properties of liquid 1-hexene at high pressures., Ul'trazvuk i fiziko-khimicheskie svoistva veshchestva (1971) 215–225.

[142] B. N. Kireev, N. F. Otpushchennikov, Experimental Investigation of the Sound Velocity in Some Olefins on the Saturation Curve, Ul'trazvuk i fiziko-khimicheskie svoistva veshchestva (1972) 47–53.

[143] S. Partharasathy, M. Pancholy, A. F. Chhapgar, Ultrasonic absorption in some homologous series of organic liquids, Nuovo Cimento Ser. 10 10 (1958) 111–131. https://doi.org/10.1007/BF02859610.

[144] G. Tardajos, M. Diaz Pena, A. Lainez, E. Aicart, Speed of sound in and isothermal compressibility and isobaric expansivity of pure liquids at 298.15 K, J. Chem. Eng. Data 31 (1986) 492–493. https://doi.org/10.1021/je00046a031.

[145] Z. Wang, A. Nur, Ultrasonic velocities in pure hydrocarbons and mixtures, J. Acoust. Soc. Am. 89 (1991) 2725–2730. https://doi.org/10.1121/1.400711.

[146] M. Zábranský, V. Růžička, Heat Capacity of Liquid n -Heptane Converted to the International Temperature Scale of 1990, J. Phys. Chem. Ref. Data 23 (1994) 55–61. https://doi.org/10.1063/1.555944.

[147] B. Kalinowska, W. Wóycicki, Heat capacities and excess heat capacities of (an alcohol + an unsaturated hydrocarbon) I. (Propan-1-ol + n-hex-1-ene), J. Chem. Thermodyn. 17 (1985) 829–834. https://doi.org/10.1016/0021-9614(85)90075-8.

[148] R. Sabbah, A. Xu-wu, J. S. Chickos, M. L. P. Leitão, M. V. Roux, L. A. Torres, Reference materials for calorimetry and differential thermal analysis, Thermochim. Acta 331 (1999) 93–204. https://doi.org/10.1016/s0040-6031(99)00009-x.

[149] J. P. McCullough, H. L. Finke, J. F. Messerly, S. S. Todd, T. C. Kincheloe, G. Waddington, The Low-Temperature Thermodynamic Properties of Naphthalene, l-Methylnaphthalene, 2-Methylnaphthalene, 1,2,3,4-Tetrahydronaphthalene,trans-Decahydronaphthalene and cis-Decahydronaphthalene, J. Phys. Chem. 61 (1957) 1105–1116. https://doi.org/10.1021/j150554a016.

[150] T. B. Douglas, G. T. Furukawa, R. E. McCoskey, A. F. Ball, Calorimetric properties of normal heptane from 0 degrees to 520 degrees K, J. Res. Natl. Bur. Stand. (U. S.) 53 (1954) 139–153. https://doi.org/10.6028/jres.053.017.

[151] B. Kalinowska, J. Jedlińska, W. Wóycicki, J. Stecki, Heat capacities of liquids at temperatures between 90 and 300 K and at atmospheric pressure, J. Chem. Thermodyn. 12 (1980) 891–896. https://doi.org/10.1016/0021-9614(80)90035-X.

[152] A. G. Akhmedov, M. F. Efendiev, B. M. Mirzoev, Temperature dependence of the heat capacity of liquid alkenes, Izv. Vyssh. Uchebn. Zaved. Neft Gaz 30 (1987) 62–65.

[153] L. Cailletet, E. Mathias, Recherches sur la densité de l'acide sulfureux à l'état de liquide et de vapeur saturée, J. Phys. Theor. Appl. 6 (1887) 414–426. https://doi.org/10.1051/jphystap:018870060041401.

[154] M. Thol, G. Rutkai, A. Köster, R. Lustig, R. Span, J. Vrabec, Equation of State for the Lennard-Jones Fluid, J. Phys. Chem. Ref. Data 45 (2016) 023101. https://doi.org/10.1063/1.4945000.

[155] M. L. McGlashan, C. J. Wormald, Second virial coefficients of some alk-1-enes, and of a mixture of propene + hept-1-ene, Trans. Faraday Soc. 60 (1964) 646–652. https://doi.org/10.1039/tf9646000646.

[156] R. Span, W. Wagner, On the extrapolation behavior of empirical equations of state, Int. J. Thermophys. 18 (1997) 1415–1443. https://doi.org/10.1007/BF02575343.

[157] E. Grüneisen, Theorie des festen Zustandes einatomiger Elemente, Ann. Phys. 344 (1912) 257–306. https://doi.org/10.1002/andp.19123441202.

[158] V. Arp, J. M. Persichetti, G. Chen, The Grüneisen Parameter in Fluids, J. Fluids Eng 106 (1984) 193–200. https://doi.org/10.1115/1.3243100.

[159] G. Venkatarathnam, L. R. Oellrich, Identification of the phase of a fluid using partial derivatives of pressure, volume, and temperature without reference to saturation properties, Fluid Phase Equilib. 301 (2011) 225–233. https://doi.org/10.1016/j.fluid.2010.12.001.

[160] R. Span, R. Beckmüller, S. Hielscher, A. Jäger, E. Mickoleit, T. Neumann, S. M. Pohl, B. Semrau, M. Thol, TREND. Thermodynamic Reference and Engineering Data 5.0, Lehrstuhl für Thermodynamik, Ruhr-Universität Bochum, Bochum., 2020.

[161] E. W. Lemmon, I. Bell, M. L. Huber, M. O. McLinden, NIST Standard Reference Database 23: Reference Fluid Thermodynamic and Transport Properties-REFPROP, Version 10.0, National Institute of Standards and Technology, Gaithersburg, 2018.